AAPS PharmSciTech (2022) 23:230
https://doi.org/10.1208/s12249-022-02377-8

RESEARCH ARTICLE

# Mannose-Anchored Nano-Selenium Loaded Nanostructured Lipid Carriers of Etravirine for Delivery to HIV Reservoirs

**Satish Rojekar[1] · Leila Fotooh Abadi[2] · Rohan Pai[3] · Mahendra Kumar Prajapati[1] · Smita Kulkarni[2] · Pradeep R. Vavia[1]**

Received: 3 May 2022 / Accepted: 25 July 2022 / Published online: 17 August 2022


## Abstract

The present investigation aims to develop and explore mannosylated lipid-based carriers to deliver an anti-HIV drug, Etravirine (TMC) and Selenium nanoparticles (SeNPs), to the HIV reservoirs via the mannose receptor. The successful mannosylation was evaluated by the change in zeta potential and lectin binding assay using fluorescence microscopy. Electron microscopy and scattering studies were employed to study the structure and surface of the nanocarrier system. The presence of selenium at the core-shell of the nanocarrier system was confirmed by X-ray photoelectron spectroscopy and energy dispersive X-ray analysis. Further, the *in vitro* anti-HIV1 efficacy was assessed using HIV1 infected TZM-bl cells followed by *in vivo* biodistribution studies to evaluate distribution to various reservoirs of HIV. The results exhibited higher effectiveness and a significant increase in the therapeutic index as against the plain drug. The confocal microscopy and flow cytometry studies exhibited the efficient uptake of the coumarin-6 tagged respective formulations. The protective effect of nano selenium toward oxidative stress was evaluated in rats, demonstrating the potential of the lipidic nanoparticle-containing selenium in mitigating oxidative stress in all the major organs. The *in vivo* biodistribution assessment in rats showed a 12.44, 8.05 and 9.83-fold improvement in the brain, ovary, and lymph node biodistribution, respectively as compared with plain TMC. Delivery of such a combination via mannosylated nanostructured lipid carriers could be an efficient approach for delivering drugs to reservoirs of HIV while simultaneously reducing the oxidative stress induced by such long-term therapies by co-loading Nano-Selenium.

**Keywords** Mannosylation · HIV infection · Nanostructured lipid carriers · Etravirine · Nano Selenium

## Abbreviations

| | |
|---|---|
| TMC | Etravirine |
| SeNPs | Selenium nanoparticle |
| HIV | Human immunodeficiency virus |
| HAART | Highly active anti-retroviral therapy |
| AIDS | Acquired immuno-deficiency syndrome |
| TMC-Se-M-NLC | Mannosylated etravirine and selenium loaded nanostructured lipid carrier |
| ARVs | Antiretrovirals |
| SeNPs | Selenium nanoparticle |
| ROS | Reactive oxygen species |
| RES | Reticuloendothelial system |
| $CD4^+$ | Cluster of differentiation 4 |
| SLN | Solid lipid nanoparticle |
| DESE | Double emulsion solvent evaporation |
| GMS | Glyceryl monostearate |
| PDI | Polydispersity Index |
| GSH | Glutathione |
| SOD | Superoxide dismutase |
| MDA | Malondialdehyde |
| LPO | Lipid peroxidation |

✉ Pradeep R. Vavia
pr.vavia@ictmumbai.edu.in

[1] Department of Pharmaceutical Sciences and Technology, Institute of Chemical Technology, Mumbai 400 019, India

[2] Department of Virology, Indian Council of Medical Research, National AIDS Research Institute, Pune 411 026, India

[3] Shobhaben Pratapbhai Patel School of Pharmacy & Technology Management, SVKM's NMIMS, V.L. Mehta Road, Vile Parle (W), Mumbai 400 056, India

## Introduction

AIDS is currently among the most severe public health challenges in the world and is caused by HIV. Globally, around 38 million people were infected with HIV/AIDS in 2019 [1]. A major clinical challenge in the treatment of HIV/AIDS in several of these infected patients has been the lack of therapeutic agents or their accessibility. Even though novel drug delivery technologies are continually being developed, the effective delivery of these technologies for reaching the underlying disease within the macrophages still needs validation [2, 3]. Based on growing literature, it has been demonstrated that the nanocarrier mannosylation increases uptake by macrophages in the target tissues or organs [4]. Moreover, the concern of toxicity of the administered substances can be reduced by focusing on enhanced uptake, which has been reported to require smaller doses of these therapeutic agents, enough to elicit a clinical response. Researchers have formulated mannosylated polymeric micelles for efficient siRNA delivery into macrophages [5]. Bhavin *et al*. have developed mannosylated PLGA nanoparticles that improve brain bioavailability [6]. Also, the scientists have evaluated the different novel drug delivery approaches in combination with mannosylation to improve selective macrophage uptakes, such as a polymeric nanoparticle, polysaccharide-based vaccine, liposome, niosome, NLC, dendrimer, solid lipid nanoparticles, chitosan nanoparticles, and gelatin nanoparticles.

Structurally, nanostructured lipid carriers (NLCs) are a blend of solid lipid and oil, thus resulting in an imperfect matrix structure [7, 8]. Such an arrangement significantly increases the drug-loading capacity of the NLC when compared with lipid NPs composed of only the solid lipid. In addition, NLCs are less likely to exhibit premature release of the drug during the storage owing to their higher capability for drug retention [9, 10]. The mannose receptor (MR), a trans-membrane glyco-protein belonging to the family of C-type lectin, is predominantly expressed on macrophages, dendritic cells (DCs) of most tissues, and also lymphatic or liver endothelial cells [11]. The extracellular region of MR presents 8 carbohydrate recognition domains (CRDs) which bind to sugars such as mannose and fructose with superior affinity [2]. The MR on macrophages interacts with pathogens and microbes that are coated with mannose-containing structures by way of host molecular mimicry [2, 12, 13]. SeNPs are potent nutritional anti-oxidants that exhibit their biological effects after incorporating into selenoproteins, which regulate the crucial balance of reactive oxygen species (ROS), and redox status in most tissues and organs.

Moreover, dietary selenium was reported to strongly influence inflammation and immune responses [14, 15]. Several clinical studies have strongly demonstrated the link between the deficiency of selenium and the progression of AIDS or even its mortality [16]. Several randomized controlled trials have shown that selenium supplementation has improved $CD4^+$ cell counts [14]. Micronutrient interventions aim to enhance the count of $CD4^+$ cells, reduce opportunistic infections, decrease HIV viral load, and reduce intracellular oxidative stress [17]. Etravirine (TMC), which was approved in 2008, is the first of the second generation non-nucleoside reverse transcriptase inhibitors (NNRTIs) for treating NNRTI resistant HIV1 infection [18, 19]. The major hurdle for TMC therapy is poor patient compliance because of frequent dosing and limited oral bioavailability attributable to its highly hydrophobic nature [20].

Thus, the current manuscript aims to develop and characterize a mannosylated nanostructured lipid carrier to simultaneously deliver TMC and SeNPs to the macrophage reservoirs in order to enhance therapeutic efficacy while also countering oxidative stress associated with the anti-HIV therapy.

## Materials and Methods

### Materials

TMC was generously gifted from Hetero Pharma, Hyderabad, India. Concanavalin A (Con A), N-[1-(2, 3-Dioleoyloxy) propyl]-*N*,*N*,*N*-trimethyl ammonium chloride (DOTAP), Dichloromethane, stearyl amine, methanol, ethyl acetate and acetonitrile were acquired from Sigma-Aldrich, India. Dulbecco's modified Eagle medium (DMEM), Roswell Park Memorial Institute (RPMI) 1640 medium, fetal bovine serum (FBS), Trypsin-EDTA 0.05% w/v, penicillin-streptomycin (pen-strep), and HEPES (1M) were obtained from the Gibco, USA. Dimethyl sulfoxide (DMSO) was obtained from Fisher Scientific, Pittsburgh, PA. Sigma-Aldrich, USA, provided 3-(4,5dimethyl thiazole-2-yl)-2, 5-diphenyl tetrazolium bromide (MTT).

### Preparationand Development of Cationic TMC-se-NLCs

The cationic-charged TMC-Se-NLCs were developed using a widely reported double-emulsion solvent-evaporation technique described previously [1, 21]. Concisely, 2 mg of the SeNPs was dispersed in 1000 µL of deionized water. Further, in a mixture of 10 mL 1:1 v/v DCM:ethyl acetate, TMC (10 mg), Softemul®-SE (100 mg), Capmul® MCM (100 mg), Span® 60 (50 mg), and DOTAP (30 mg) were dissolved. Then, the pre-formed aqueous dispersion of SeNPs was added gradually to the mixture of DCM:ethyl acetate phase under Ultraturrax (IKA® Ultra-Turrax® dispersers, IKA, India), stirring at 18,000 rpm for 30 s to produce a

w/o (primary emulsion) which was further added drop-wise to a 50 mL aqueous solution of 1% w/v Lutrol® F127 under Ultraturrax stirring at 12,000 rpm for 60 s. This coarse emulsion particle size was further reduced by using an ultrasonic cell disruptor (Dakshin Instruments, India) with a 10 mm diameter probe, which functioned at (200 W) for 5 min 5 s and off for 3-s durations. The subsequent w/o/w emulsion was kept under constant stirring on the magnetic stirrer (IKA Magnetic Stirrers, RH basic white, IKA, India) at room temperature to evaporate DCM: Ethyl acetate (5–6 h). The developed cationic TMC-Se-NLC was confirmed by the change in zeta potential. This was further used for the development of mannosylated TMC-Se-M-NLC. The lipid to mannose ratio and incubation time on zeta potential were determined to optimize the TMC-Se-M-NLC.

## Preparation and Development of Mannosylated TMC-se-M-NLCs

After the cationic NLC, a solution of d-mannose in PBS buffer (10 µg/mL) was added to the cationic TMC-Se-NLCs dispersion to achieve a nanoparticle lipid: mannose ratios of (1:0.1, 1:0.25, 1:0.5, 1:1, and 1:2). The dispersion was incubated at 37°C for 24 h. Further, it was dialyzed to remove unbound mannose (Supplementary Material S1). TMC-Se-M-NLC was filled into the freeze-drying vials. Then it was frozen in the deep freezer (Labtop® Micro Controller based Vertical Biofreeze, India) at – 60°C for 12 h and followed by the freeze-drying (VirTis AdVantage 2, Benchtop Freeze Dryer, New York, USA), according to the following protocol: Primary drying for 22 h at a shelf temperature maintained at – 10°C, followed by secondary drying at shelf temperature of 10°C for 2 h and a vacuum pressure of 100 mTorr). After completion, freeze-dried powder was collected and utilized for all the solid-state characterization, including FTIR, DSC, XRD, X-ray photoelectron spectroscopy (XPS), and transmission electron microscopy (TEM-EDAX). The concanavalin A (10 µg/mL) solution was used as a standard solution for further optimization. The concanavalin A binding assay was performed to determine mannose-binding with the nanoparticles that were confirmed by spectrofluorimeter Synergy H1 Hybrid Multi Mode Reader, BioTek®, USA, in the range 300–500 nm, at an excitation wavelength of 280 nm. The effect of time (30 min, 1, 2, 4, 8, and 24 h) and nanoparticle lipid:mannose ratio (1:0.1, 1:0.25, 1:0.5, 1:1, and 1:2) were optimized by fluorimetric emission. Unbound concanavalin A concentration was determined by comparing fluorescence intensity with standard concanavalin A at 335 nm. % Concanavalin A binding was calculated using Eq. 1 [22].

$$\%\mathbf{CON\ binding} = \frac{(\mathbf{[CON]total} - \mathbf{[CON]unbound})}{\mathbf{[CON]\ total}} x100 \quad (1)$$

## Interaction of Nanoparticles with d-mannose

### Fluorescence Spectrophotometry

The interaction of concanavalin A with the TMC-Se-M-NLCs was analyzed using fluorescence spectroscopy. The concanavalin A binding is directly proportional to the mannose-binding to the nanoparticle surfaces (lectin binding assay). The binding of concanavalin A measured the fluorescence quenching of tryptophan by concanavalin A to the mannosylated nanoparticles [22]. A known quantity of concanavalin A was dissolved in PBS for the fluorescence quenching experiments to form a standard solution (10 ppm). The excitation wavelength used was 280 nm for selectively exciting the tryptophan residues, whereas the emission was recorded in-between the range of 300–500 nm by a fixed excitation and an emission slit width of 5 nm. The unknown concentration of the test solution of concanavalin A was calculated by comparing fluorescence intensity at 300 nm of the standard solution with the unknown concentration by using the Eq. (2) given below:

$$\text{Concentration of unknown concanavalin A sample} = \frac{\text{Ft} * \text{Cs}}{\text{Fs}} \quad (2)$$

Ft: Fluorescence intensity of test sample
Cs: Known amount of concanavalin A in standard solution
Fs: Fluorescence intensity of standard concanavalin A solution

### Molecular Docking

The Maestro (Schrodinger, LLC, New York, USA, 2008) implemented the Glide molecular docking protocol to understand the interaction between d-mannose and GMS/DOTAP/TMC/d-mannose. The crystal structure of d-mannose with the code 5XTS was downloaded from the protein data bank (PDB) and used for the docking studies. Sitemap analysis was performed to determine the possible active sites on d-mannose, and Grids were generated using sites defined by sitemap analysis. The ligand structures GMS/DOTAP/TMC/d-mannose were constructed using the build option within the Maestro version. However, with the help of the Ligprep facility, the low-energy 3D conformations were created for each ligand through energy minimization steps with a dielectric constant of 1 and docked into the active site using the standard precision mode of Glide docking

protocol. Docking calculations were performed using Glide genetic algorithm. Interactions were characterized based on a G score (most negative interaction energy).

## Characterization of Developed TMC-se-M-NLC

### Particle Size, Zeta Potential, and Polydispersity Index Measurements

Prior to particle size analysis, TMC-Se-M-NLCs were appropriately diluted up to 10-times by Milli-Q water. Then samples were in triplicate with a scattering angle of 90° and a temperature of 25°C for particle size analysis and the polydispersity index (PDI). However, the zeta potential of the NLC preparations were directly placed in the electrophoretic cells. The zeta potential was analyzed in triplicate using Zeta Sizer Nano ZSP (Malvern, USA).

### Drug-Loading and Encapsulation Efficiency

TMC-Se-M-NLCs were assessed for % drug-loading and the EE. In brief, 2 mL of TMC-Se-M-NLCs were centrifuged at 20°C for 2 h at 35,000 rpm using Sorvall WX Ultra 100, Thermo Scientific, USA. Then the supernatant was collected and filtered using a syringe filter (0.22 µm) to remove the excess or unwanted residues of lipids. Further appropriate dilution was done using methanol, and then the un-entrapped drug was analyzed by the developed HPLC method as reported in Supplementary Information S1. The % EE and % drug loading were calculated using the following Eqs. 4 and 5;

$$\%EE = \frac{\boldsymbol{W\ total - W\ drug}}{\boldsymbol{W\ total}} \times 100 \quad (4)$$

$$\text{Drug loading } (\%) = \frac{\boldsymbol{W\ drug}}{\boldsymbol{lipid}} \times 100 \quad (5)$$

*W*drug is TMC (drug) in the supernatant; *W*total is total TMC in the formulation.

### Small Angle Neutron Scattering

The small angle neutron scattering (SANS) was executed at the SANS-diffractometer at the Bhabha Atomic Research Centre, Mumbai, India, in the Guide Tube Laboratory of the Dhruva Reactor. SANS generates valuable information about the scattering particles' shape and size on the length scale of 10–1000 Å [23]. The formulations were appropriately prepared in a stabilizer solution made in deuterated water ($D_2O$, double filtered). The rest of the procedure was similar to the TMC-Se-M-NLCs preparation section. The protocol followed for the analysis was the same as described previously in the literature and the data points obtained were fitted using SASfit into appropriate models [24].

### Transmission Electron Microscopy

TMC-Se-M-NLCs were evaluated for morphology and elemental composition by using the transmission electron microscopy (TEM-EDAX) from the Tecnai 20, Philips, Netherlands. A 100 µL of diluted NLC nanodispersion was uniformly positioned on the carbon coated grid # 300 mesh grid, Ted Pella, Inc, Redding, Canada, and dehydrated and dried subsequently with the addition of 2% w/v uranyl acetate. Then it was dried at 28°C prior to mounting, followed by recording images at an accelerating voltage of 120 keV.

### X-Ray Photoelectron Spectroscopy

The protocol followed for the sample preparation for the X-ray photoelectron spectroscopy (XPS) analysis was as described previously [21]. Briefly, the dried samples were analyzed at a maximum energy of 1486.6 eV by a 600 W (monochromatic Al-Kα X-ray) source within an XPS (Kratos Analytical, Shimadzu, Japan). The binding energy among elements was recorded for all samples from 0 to 1400 eV, while the resulting spectra were recorded at 50 W excitation energy.

## *In Vitro* Drug Release Study

The free TMC solution and the NLCs were assessed for *in vitro* drug release for 24 h through the dialysis method (dynamic) [25]. TMC-Se-M-NLC's equivalent to 5 mg of TMC was added to the end sealed dialysis membrane by Hi-Media, India. Dialysis bags were clipped on both sides and then placed in 200 mL of pH 7.4 phosphate buffer, with a tween 80 (1% w/v) and sodium azide (0.01% w/v). The whole setup was kept at 37°C on the magnetic stirrer at 100 rpm [25, 26]. Then, 2 mL of the fluid was drawn at mentioned time intervals, followed by analysis by the HPLC method reported in Supplementary Information S1. The dissolution media volume was maintained by replacing the equivalent volume.

## Serum Stability

TMC-Se-M-NLCs were assessed for *in vitro* serum stability for protein binding and monitored change in particle size for 5 days. In brief, 1 mL TMC-Se-M-NLCs nanodispersion was incubated in 5 mL human plasma (10% v/v diluted in PBS), PBS, and FBS (100% v/v) for 5 days at 37 ± 2°C. The aliquot of 100 µL was withdrawn at 1, 2, 3, 4, and 5 days and then diluted appropriately with deionized water, and particle size was analyzed by Malvern Zeta Sizer.

## Cell Line

National Institutes of Health, AIDS Research and Reference Reagent Program (NIH ARRRP, USA) provided the TZM-bl cell line that was cultured in the DMEM medium added with FBS (10% v/v), penicillin (100 U/mL), l-glutamine (2 mM), streptomycin (100 µg/mL), and HEPES buffer (25 mM) solution incubated in 5% v/v $CO_2$ at 37°C.

## Virus Stocks Propagation

The virus stocks were prepared as previously described in the literature [25, 27]. HIV-1 primary isolates, $HIV1_{VB28}$ (CCR5 tropic, Subtype C, ICMR-NARI, India) and $HIV1_{UG070}$ (CXCR4 tropic, Subtype D, NIH ARRRP, USA), were used. The virus stocks were propagated in 500 µL of pHA-p activated human peripheral blood mononuclear cells (PBMC) [27]. HIV-1 p24 antigen detection kit, Advanced Bioscience Laboratories, Inc, USA, was used to determine the viral growth using the ELISA method. The cell-free culture supernatant was filtered, collected and stored at – 80°C. The $TCID_{50}$ (50 % Tissue-culture infective dose) was determined after titrating the virus stocks.

## *In Vitro* Cytotoxicity

In brief, the TZM-bl cells, $10^4$ cells/well, were plated in 96-well plates and incubated in a 5% v/v $CO_2$ chamber (Stoelting, USA) overnight at 37°C. Then the next day, the medium was exchanged with a serum free medium. Further, the test substances (TMC, SeNPs, TMC-Se-NLCs and TMC-Se-M-NLCs) were diluted serially, added to wells, and incubated for 48 h. Afterward, 20 µL of (MTT, 5 mg/mL) was added to each well and incubated for 4 h. Then, 200 µL DMSO was used for assay termination, which dissolved the formazan crystals, and a plate was analyzed at 550 nm and 630 nm. The $CC_{50}$ (concentration showing 50% cytotoxicity) was determined using a non-linear dose-response regression analysis [27].

## Assessment of Potential Anti-HIV1 Activity

TZM-bl Cells, $10^4$ cells/well in D10 (DMEM added with 10% heat inactivated FBS), were plated in the 96-well microplates. On a subsequent day, 400 TCID 50/mL value of the pre-tittered virus/s were used for cells infection. The virus stocks of $HIV1_{VB28}$ or $HIV1_{UG070}$ (pre-titrated 400 TCID 50/mL) were incubated in a humidified 5% v/v $CO_2$ chamber for 2 h at 37°C [25, 27]. Sub-toxic concentrations (two-fold serial dilutions) of the TMC-Se-M-NLCs, TMC solution, and SeNPs were added to the infected cells and incubated for 48 h. For the control samples, the uninfected TZM-bl cells were used. After 48 h of incubation, Britelite plus reagent, Perkin Elmer, USA, was added and the relative luminescence units (RLU) were measured by the Luminometer, Victor 3, Perkin Elmer, USA. The % inhibitions were measured and calculated, and the results were represented as $IC_{50}$ value (concentration inhibiting 50% of the viruses) using the LUC software (version 04.4). The therapeutic index ($TI = CC50/IC50$) was calculated and compared with a standard drug control (TMC).

## TZM-bl Cellular Uptake/Internalization Study

### Cou-6 Tagged TMC-se-M-NLCs Preparation Method

For the visualization of the NLC, the TMC-Se-M-NLC were prepared using Coumarin-6 (Cou-6) by dissolving Cou-6 (0.01% w/v) into the oil-phase (The organic phase (DCM:ethyl acetate,1:1 v/v). The NLC during the preparation of TMC-Se-M-NLC and utilized for the following experiments.

### Confocal Laser Scanning Microscopy

The TZM-bl cells were seeded at $0.1 \times 10^6$/well on the cover-slips and then incubated at 37°C in a 5% v/v $CO_2$ overnight. Subsequently, D10 (DMEM supplemented with 10% v/v heat-inactivated FBS) was replaced with 0.02 mg/mL of Cou-6 tagged TMC-Se-M-NLC in serum free DMEM media [volume was 200 µL/well]. The medium was discarded after 2 h of treatment, and then cells washing was done and immobile using the paraformaldehyde (4% v/v in PBS pH 7.4). Further, the cells were permeabilized with 0.5 mL/well Triton™ X-100 (0.1% PBS) prepared in PBS for 3 min. Subsequently, the cytoskeleton and the cell nuclei were stained by 5 µL/well (DAPI, 1 ng/mL) with the 2 µL/well Texas Red-Phalloidin (Invitrogen, 6.6 µM), respectively. ProLong™ Gold Antifade Mountant (Thermofisher Scientific, USA) was used to mount the slides after staining. Confocal laser scanning microscopy (CLSM), Leica Microsystems at 60× magnification with oil was used to take cell images.

### Flow Cytometry Evaluation

The flow cytometry evaluated the cellular internalization of the Cou-6-tagged TMC-Se-M-NLCs [25, 27]. Concisely, $0.2 \times 10^6$ TZM bl cells in D10 were plated in the 96-well plates and incubated at 37°C, 5% v/v $CO_2$ for the 24 h. The following day, the culture media was replaced by serum free DMEM media, including the 0.02 mg/mL Cou-6 tagged TMC-Se-M-NLCs and further incubated at 37°C for 15, 30, 45, 60, and 120 min to measure the cellular uptake of TMC-Se-M-NLCs. The cell washing and detaching were performed using the 0.25% v/v Trypsin EDTA. The cells were re-suspended in PBS (1×) for uptake evaluation.

FACSAria™ Fusion flow cytometer, Becton Dickenson, was used to determine cellular uptake, and the data were analyzed with FACS Diva software.

### *In vivo* Acute Toxicity and Anti-Oxidant Studies

The protective effect of SeNPs containing nanoformulation against intracellular oxidative stress induced by the doxorubicin hydrochloride (Dox HCl) was assessed on Wistar rats weighing 200 ± 20 g (approval number: PBRI/PN/2020104 from Pinnacle Biomedical Research Institute, Madhya Pradesh, India). The rats were housed in standard temperature, humidity, and light (25 ± 2°C; 12 h cycle). The rats were fed with a standard pellet diet as well as water. The animals were grouped into positive control groups, negative control groups, as well as the preventive group, all containing six animals each. The animals were adjusted to the housing environment for 14 days prior to the study. The animals were dosed on the 1st day. The positive control group received 5 mg/kg intraperitoneal doxorubicin hydrochloride, while the negative control group was intravenously administered saline.

On the other hand, the preventive group received TMC-Se-M-NLCs at 2.5 mg/kg of body weight by the intravenous route. After 1 h of initial dosing, the rats in the preventive group intraperitoneally received 5 mg/kg/day of Dox-HCl in order to provoke oxidative stress. Around 500 µL of blood was withdrawn from the anesthetized animals on 1, 7, and 21 days and evaluated for serum biochemistry. The markers for oxidative stress were studied at study termination from the vital organs, which were cleaned using ice-cold saline before homogenizing them using 0.1 M, pH 7 Tris-HCl buffer. Histopathology studies also assessed the organs to evaluate any damage in the organs. For *In Vivo* Acute Toxicity and Anti Oxidant Studies, The animal ethics committee from Pinnacle Biomedical Research Institute (PBRI), Madhya Pradesh, India approved the protocol numbered PBRI/ PN/2020104 and for *In Vivo* Biodistribution Study the Institutional Animal Ethics Committee (IAEC) of Institute of Chemical Technology, Mumbai approvedthe protocol numbered ICT/IAEC/2019/P06.

### *In vivo* Biodistribution

Eighteen rats (weight 150–200 g) were divided into three groups; each group consisting of 6 animals and fasted for 6–7 h before the dosing (Protocol number: ICT/IAEC/2019/P06). The saline, 2.5 mg/kg of TMC-Se-M-NLCs and 2.5 mg/kg of TMC in DMSO solution were intravenously administered through the tail vein. Then rats were sacrificed at corresponding time points of 1 h, and 24 h ($n = 3$). The drug in the concerned organs was evaluated by HPLC (bioanalytical method) reported in Supplementary Information S1 [25]. In brief, organs were accurately weighed and homogenized using (1:2 w/v of organ: PBS) pH 7.4 by RQ-Remi Tissue Homogenizer, 127A/D, India. The SALLE method was used to extract TMC and the internal standard (Tamoxifen citrate, TMX) from the homogenized organs as described in the literature [28, 29].

## Statistical Analysis

The results were analyzed statistically by one-way analysis of variance (ANOVA) following the Bonferroni *t* test, $p < 0.05$ considered as a level of significance while comparing between groups wherever applicable using GraphPad Prism software.

## Results and Discussion

### TMC-SE-M-NLC Development and Characterization

#### Effect of Cationic Lipid (DOTAP) Concentration on Zeta Potential

The TMC-Se-NLCs have been reported and characterized previously [21]. Initially, TMC-Se-NLCs had an anionic zeta potential of − 18.47 mV. Further, during the development of cationic TMC-Se-NLCs, various concentrations of DOTAP were tried (0.005–0.03 mmol). When the DOTAP concentration was subsequently increased from 0.005 to 0.03 mmol, there was a considerable increase in the positive charge on the TMC-Se-NLCs. The change in zeta potential with respect to cationic lipid concentration is shown in Table I. This could be due to the positive charge present in the DOTAP structure and its composition [30–32]. Further, the optimized TMC-Se-NLCs were used to develop the mannosylated TMC-Se-M-NLCs.

#### Effect of d-Mannose Concentration on Zeta Potential (Lipid to Mannose Ratio)

For the mannosylation of the TMC-Se-NLCs, different lipid to d-mannose ratios was tried (1:01 to 1:2 w/w) at a fixed incubation time of 24 h and a constant temperature of 37°C. The lipid was kept constant during the mannosylation; however, d-mannose concentration was varied. It was observed that when the d-mannose concentration increased

**Table I** Effect of Cationic Lipid Concentration on Zeta Potential of TMC-Se-NLCs

| Cationic lipid concentration (mg) | Zeta potential (mV) |
|---|---|
| 0.005 | − 5.325 |
| 0.01 | − 1.943 |
| 0.03 | 10.81 |

**Table II** Effect of Mannose Concentration on Zeta Potential (Lipid to Mannose Ratio) of the TMC-Se-M-NLCs

| Lipid to mannose ratio (mg) | Zeta potential (mV) |
|---|---|
| 1:0.1 | − 7.82 |
| 1:0.25 | − 21.24 |
| 1:0.5 | − 26.75 |
| 1:1 | − 39.03 |
| 1:2 | − 40.73 |

**Table III** Effect of Incubation Time on Zeta Potential of the TMC-Se-M-NLCs

| Incubation time (h) | Zeta potential (mV) |
|---|---|
| 1 | − 1.73 |
| 2 | − 4.92 |
| 4 | − 14.42 |
| 8 | − 19.52 |
| 24 | − 34.5 |

from 1:0.1 to 1:2, a significant ($p < 0.0018$) increase in the negative zeta potential was observed, as shown in Table II [3, 33]. The considerable change in the charge onto nanoparticles could result due to the deposition of d-mannose on the nanoparticle surfaces. Such a difference in the charge was also witnessed for the lipid nanoparticles after their functionalization with d-mannose in reported literature [33]. This could suggest the binding of d-mannose to the cationic TMC-Se-NLCs, thereby confirming the mannosylation of the TMC-Se-NLCs and converting it to the TMC-Se-M-NLCs. Zeta potential and its magnitude is also indicative of colloidal stability. Generally accepted particles with a zeta potential between – 25 mV and + 25 mV usually possess high stability. In contrast, particulate dispersions with low zeta potential would eventually aggregate due to Van Der Waal's inter-particle interactions [34].

### Effect of Incubation Time on Zeta Potential

The effect of incubation time on the zeta potential was evaluated to confirm the degree of mannosylation of the TMC-Se-M-NLCs with respect to the incubation time. It was observed that the higher the incubation time, the higher the zeta potential, as given in Table III. The maximum zeta potential was observed at 24 h. This could be because the d-mannose would get more time to contact the nanoparticles, which would form more electrostatic bonding and show higher zeta potential values than the lower incubation time [33]. Therefore, 24 h was selected as an optimized incubation time for further development.

## Mechanism of Interaction of Nanoparticles with d-Mannose

### Fluorescence Spectrophotometry

In this present study, the physical adsorption method was employed for loading d-mannose ligand on the surface of the TMC-Se-M-NLCs. d-Mannose was successfully incorporated on the surface of the TMC-Se-NLCs by a simple incubation method [33, 35, 36]. Spectrofluorometric evaluations confirmed the anchoring of the d-mannose on the surface of the TMC-Se-NLCs (Fig. 1). The tryptophan residues (TRP at 40, 88, 109, and 182) present in the CON (Concanavalin A) monomer is responsible for its fluorescence. The binding of the d-mannose with CON via hydrophobic interactions results in a reduction in tryptophan fluorescence. A high and maximum binding of more than 75% was observed at a lipid to the d-mannose ratio of 1:0.5 (Fig. 1a and c). However, a further increase in CON concentration showed no considerable enhancement in binding (Fig. 1a and c). Incubation of nanoparticles with d-mannose (1:0.5) for 24 h revealed comparable fluorescence quenching with more than 75% binding, suggesting 24 h to be the adequate time for reaction (Fig. 1b and d).

### Molecular Docking

Based on Sitescore, sitemap 2 with the highest score was selected for docking studies. DOTAP formed the electrostatic interaction with the LEU 304 and PRO 305 and hydrophobic interactions with the GLU238 and LYS 326 residues of the mannose receptor as demonstrated in Fig. 2a and exhibited a glide score of − 1.26 kcal/mol. GMS formed a hydrogen bond with the LEU 301 and LYS 326 residue of the mannose receptor was demonstrated in Fig. 2b and exhibited a glide score of − 2.9 kcal/mol. TMC formed a hydrogen bond with LEU 301 residue of the mannose receptor, as shown in Fig. 2c, and showed a glide score of − 5.29 kcal/mol. Also, LEU 304 and PRO 355 residue were found to interact with TMC, suggesting the role of hydrophobic interaction. SER 454, HIP 455, GLU 456, ASN 457, GLY 306, and SER 307 residues of the mannose receptor strongly interacted with the ligand d-mannose (Fig. 2d), suggesting the role of hydrogen bonding interactions with the mannose receptor. In addition, GLY 305, SER 307 & 457, PRO 308, and HIP 457 residue of the mannose receptor were found to be interacting strongly with d-mannose, suggesting the role of hydrophobic interactions. This was confirmed by the higher negative glide score of − 9.20 kcal/mol of the d-mannose after interaction with the mannose receptor. Thus, the more negative G score of d-mannose could relate to a stronger affinity of ligand d-mannose with mannose receptor *in silico*.

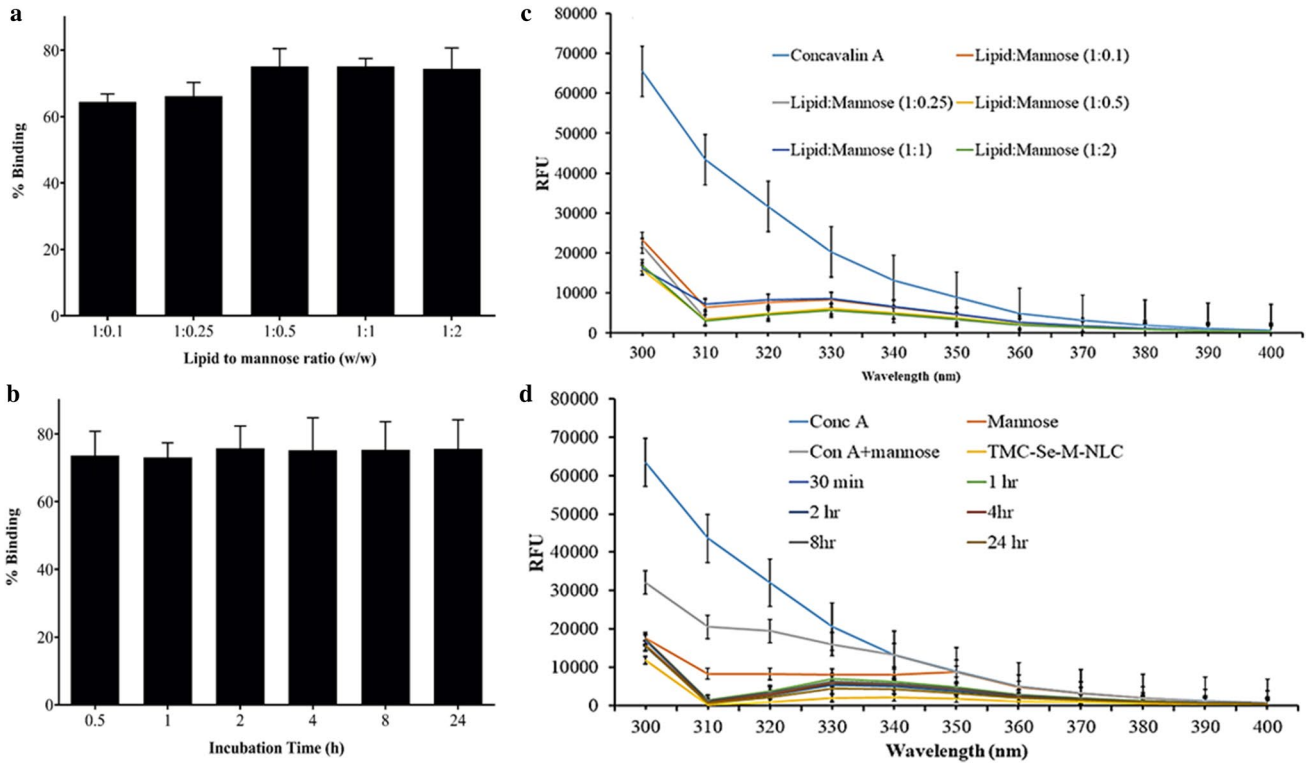


**Fig. 1** **a** Effect of lipid to mannose ratios on % d-mannose-binding to the nanoparticle and **b** effect of incubation time on the % d-mannose-binding with nanoparticle. **c** Fluorescence quenching of CON (10 µg/mL) on interaction with different lipid to mannose ratios. **d** Effect of incubation time of nanoparticles and CON incubation on CON (10 µg/mL) fluorescence

## Particle Size and Zeta Potential Evaluation

The mean particle size and PDI of the TMC-Se-M-NLCs were found to be 287 ± 15.30 nm and 0.266 ± 0.06, respectively. The data corroborates with the findings of TEM studies which also indicated a similar size range for the developed NLC. The zeta potential was − 34.5 mV, possibly due to the negatively charged hydroxyl functionalities of the d-mannose distributed at the exterior surface of the nanoparticles [33]. Moreover, the increased zeta potential of the TMC-Se-M-NLCs also improves the physical stability of the system.

## Drug Loading and Encapsulation Efficiency

The % drug loading and EE of the TMC-Se-M-NLCs were found to be 4.35% and 95.61 ± 0.86%, respectively. TMC being highly hydrophobic could have partitioned within the lipid matrix, thereby leading to a high % EE of greater than 90%. Moreover, MCT could increase hydrophobic drug encapsulation attributed to high solubility and partitioning of TMC [37, 38].

## Small-Angle Neutron Scattering

The obtained data points were fitted into particulate models using the mathematical equations.

The data were fitted and plotted as a scattering plot shown in Fig. 3. In the small angle neutron scattering (SANS) plot, lower Q($Å^{-1}$) values are referred to as Guinier-region, which gives information about the system particle size and its physical form [23]. However, the higher Q($Å^{-1}$) values are denoted as the Porod-region, which describes the shape and interparticle distance [23, 39]. The data obtained from the TMC-Se-M-NLCs fitted well in the core-shell particle models. A minute bending or deflection was noticed toward the end of the Porod-region, suggesting that the NLCs could be of the core-shell type [40]. A core-shell model may exhibit a pattern where a solid lipid core is surrounded by the stabilizer, which could form the coat or shell around the NLCs [41].

## Transmission Electron Microscopy

The transmission electron microscopy (TEM) studies of the TMC-Se-M-NLCs showed the spherical core-shell shape of

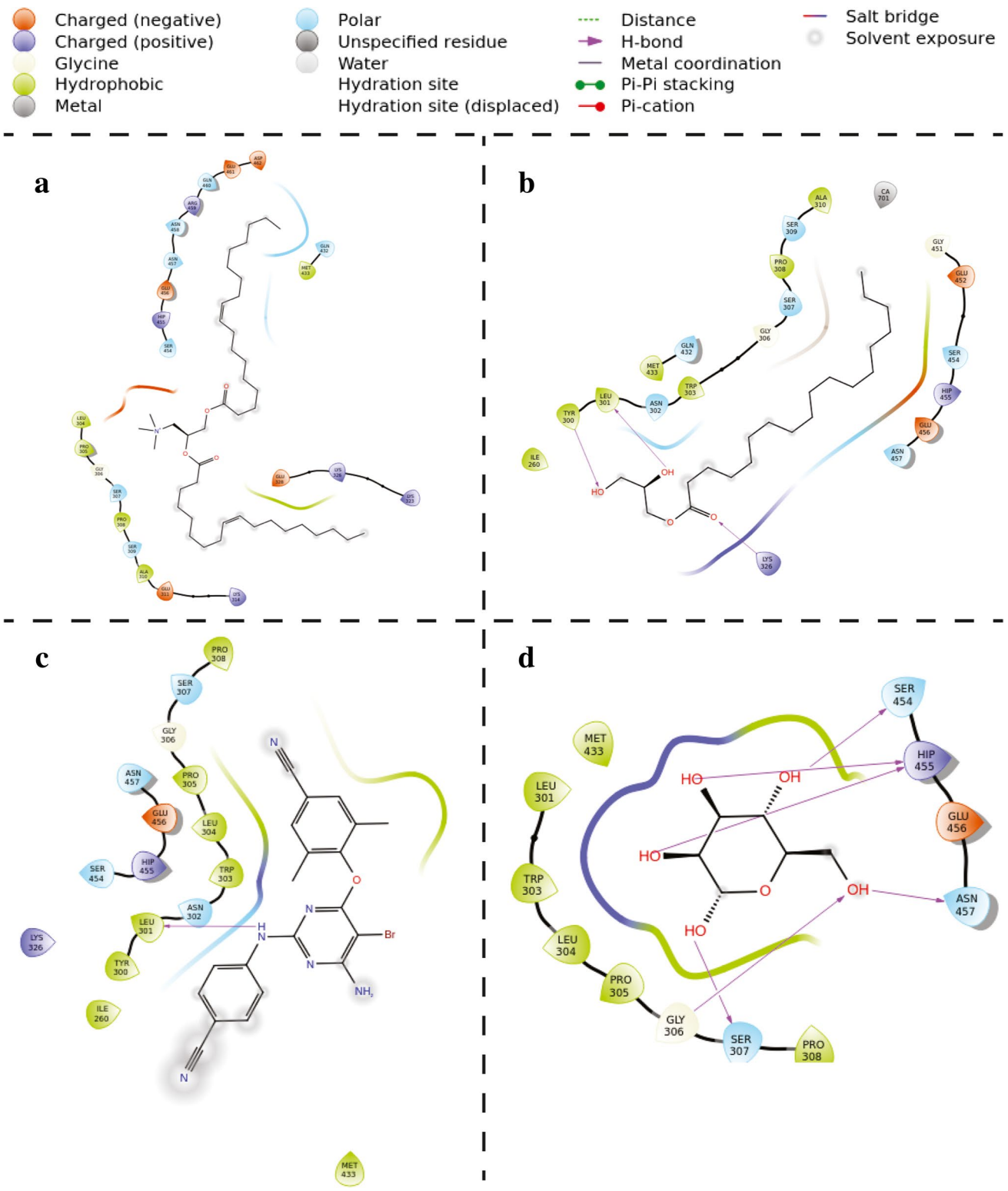


**Fig. 2** 2-D representation of Molecular docking study of mannose receptor with **a** DOTAP, **b** GMS (Softmul-SE), **c** TMC, and **d** d-Mannose

the coated mannosylated nanoparticles, as shown in Fig. 4. Further, the TEM photomicrographs demonstrated their nanometric size (Fig. 4a and b). The core-shell region of the TMC-Se-M-NLCs exhibited dark spots in the structure, indicating the presence of selenium in the nanoparticles in the nanocrystalline form (Fig. 4a). Such findings have been

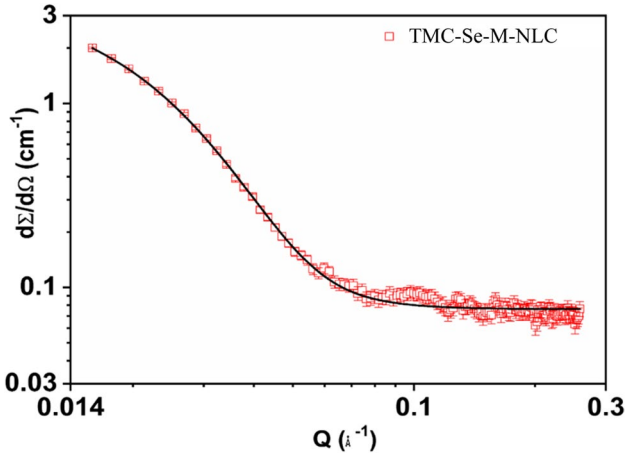


**Fig. 3** Scattering SANS plot of TMC-Se-M-NLCs showing observed and modeled data points

previously reported for the other types of metal nanoparticles like the selenium nanoparticle [42, 43]. In addition, the elemental composition of the TMC-Se-M-NLCs was also confirmed by the TEM-EDAX are shown in Fig. 4c and d [44]. The nanoparticles' EDAX spectra showed that the TMC-Se-M-NLCs were composed of nano selenium and multiple other elements present, as shown in Fig. 4c and d [45].

## X-Ray Photoelectron Spectroscopy

The characteristic peaks were found to be around 283 eV for the carbon (C1s) and 531 eV for the oxygen (O1s) states, as shown in Fig. 5a [46, 47]. This suggested the presence of several organic elements in the nanoparticulate system. However, in Fig. 5a, peaks corresponding to the selenium elemental state Se3d between 50 and 70 eV were observed. The characteristic band for the Se3d state of selenium is present as SeNPs, thereby confirming that selenium in its Se3d form could be present at the TMC-Se-M-NLCs core-shell [48]. Similar reports have been observed for other delivery systems as well, wherein the SeNPs were coated around using chitosan [38, 48]. The X-ray photoelectron spectroscopy (XPS) results corroborated sufficiently with the TEM-EDAX findings, which also suggested that the core shell of the TMC-Se-M-NLCs could be made up of the presence of SeNPs.

## *In vitro* Drug Release

The cumulative drug released was assessed using the widely reported direct dialysis method [25, 49]. In the case of the TMC solution, more than 90% of drug was found to be released at 12 h as it was not encapsulated in any release retarding material. The release thereafter was observed to plateau which could be due to the loss in the concentration gradient for TMC across the dialysis membrane. However, in the case of TMC-Se-M-NLCs, the drug release was nearly observed to be 20% at 12 h. This represented a controlled drug release potential for TMC-Se-M-NLCs for 48 h. From the initial few points, no burst release was in TMC-Se-M-NLCs (Fig. 6a). The drug may present as a homogeneous dispersion in the NLCs matrix, thus not being able to form the drug-abundant regions or pockets at the NLCs surface, subsequently in a slower release of the drug [38, 49, 50]. The TMC-Se-M-NLCs showed the sustained-release of the drug, which could be due to the diffusion of the drug particle across the lipid matrix of the NLCs [38, 51]. Similar outcomes were reported from the studies previously reported [52, 53].

## Serum Stability

TMC-Se-M-NLCs were assessed for the *in-vitro* serum stability to confirm the effect of protein binding on the particle size, thereby its colloidal stability. An initial slight increase in particle size was noted, though NLCs maintained colloidal stability during the study up to 120 h (Fig. 6b). The findings suggested that the plasma protein binding of the NLC was not an essential factor. The formulation was found to be considerably stable, owing to the steric repulsion due to the presence of polymeric stabilizer [54, 55]. This study corroborated sufficiently with the zeta potential analysis study; however, the increase in the nanoparticle's zeta potential leads to an improvement in the physical stability of the system [33].

## Cytotoxicity Determination

The percent viability of TMC, SeNPs, TMC-Se-NLCs, and TMC-Se-M-NLCs is depicted in Fig. 7a. Based on these data, the $CC_{50}$ values were calculated, which were found to be 172.5 ± 12.92 µg/mL, 20.68 ± 2.22 µg/mL, 7.08 ± 2.09 µg/mL, and 7.52 ± 0.70 µg/mL, respectively [21]. It was observed that the developed formulation was cytotoxic in comparison to drug (TMC) solution, which could be ascribed to the nanoparticulate forms. Researchers have reported previous reports wherein it has been established that nanoparticles composed of solid or crystalline matrix induce greater toxicity than those containing liquid lipid matrix [56–58].

## Evaluation of Anti-HIV1 Activity

Interestingly, the $IC_{50}$ values of TMC-Se-M-NLCs were significantly low compared to the TMC solution (Fig. 7b). The $IC_{50}$ values of TMC, SeNPs, TMC-Se-NLCs, and TMC-Se-M-NLCs against $HIV1_{VB28}$ (R5) were indicative of enhanced

anti-HIV1 activity of TMC after coating with NLCs and mannosylation.

The therapeutic index (TI) of TMC, SeNPs, TMC-Se-NLCs, and TMC-Se-M-NLCs for $HIV1_{VB28}$ and $HIV1_{UG070}$-infected TZM-bl cells were also calculated and are shown in Fig. 7c. The TI for free drug was found to be lower when compared to that of TMC-Se-M-NLCs for both the strains. Thus, the results of TI exhibit that the developed formulation had a higher therapeutic index than free TMC, which could be due to the nano-selenium and mannosylations synergistic effect [59, 60].

## Cellular Internalization and Uptake Study

### Confocal Laser Scanning Microscopy

Peculiar green puncta within the treated cells indicated an increase in the accumulation of TMC-Se-M-NLCs tagged with Cou-6 (Fig. 8a). Such an observation was not seen for free Cou-6 cells treated, confirming the internalization of TMC-Se-M-NLCs by the TZM-bl cells. Thus, these results demonstrated that TMC, after loading with TMC-Se-M-NLCs, was internalized by the cells effectively. The distinctive feature of the mannose receptor is its quick cellular internalization via an endocytosis mediated mechanism which delivers lipidic nanocarrier to the endocytic-pathway [2, 12, 61]. Moreover, mannose receptors promote the internalization of mannosylated particles. Several studies have established the efficiency of binding to the mannose receptors by conjugating a mannose to lipidic NPs [62, 63]. Nanoparticle interaction with the TZM-bl cells provides strong adhesive forces resulting from specific ligand-receptor binding and non-specific bonds such as electrostatic, steric interactions, and Van der Waals forces, resulting in higher cellular internalization of the nanoparticle [33, 64]. Cellular internalization is governed by the nanoparticle physicochemical properties such as particle size, shape and surface properties [65].

### Flow Cytometry

Analysis with flow cytometry indicated that TZM-bl cells exposed to 0.1 mg/mL, Cou-6 tagged nanoparticles exhibited that almost all test substances were taken up (99.9%) after 2 h of treatment, as shown in Fig. 8b. Thus, the obtained results confirmed that TMC, after loading with TMC-Se-M-NLCs, was internalized by the cells effectively. The *in vitro* cell uptake indicated that mannosylation could enhance the lipidic nanoparticle uptake mediated by endocytosis [61, 64]. The mannosylation of NLCs resulted in higher uptake by TZM-bl cells. Analogous behavior was already described for polymeric nanoparticles [66, 67]. Some studies have proved the efficiency of delivering via mannose receptors by tethering a d-mannose to lipidic and polymeric nanoparticles, stimulating the macrophages in the direction of a robust preventive action against the intracellular viruses or pathogens [53, 61, 68].

## *In vivo* Acute Toxicity and Anti-Oxidant Evaluation

The oxidative stress could induce cytotoxicity and chronic stress in the organs, thereby producing pro-inflammatory cytokine and could increase the level of nuclear factor-kappa B (NF-kB) [69, 70]. This would affect the HIV infection pathogenesis and could increase the replication of HIV [69]. However, several researchers have shown that synthetic and natural anti-oxidants like alpha lipoic acid, lycopene, vitamin C, and *N*-acetyl cysteine protect against anti-cancer drug-induced toxicity [71, 72]. Moreover, nano-selenium (SeNPs) exhibited an ability to shield against cellular damage, thereby retaining the intracellular anti-oxidants levels and maintaining cellular health [16, 69, 73]. It also showed that the anti-oxidant and anti-HIV activity could act synergistically to act efficiently on HIV from within the viral reservoirs [74, 75]. Thus, we have evaluated the protective potential of the SeNPs against the Dox HCl-induced stress in the rats. Dox HCl has been widely used as an anti-cancer drug to treat several cancers; however, it produces severe toxic effects. This could show the potential of the SeNPs in oxidative stress management during HIV infection by reducing the pro-inflammatory cytokines and NF-kB, thereby decreasing the HIV pathogenesis, which may improve the synergistic anti-HIV efficacy.

### Glutathione

The level of glutathione (GSH) was found to be significantly ($p < 0.001$) decreased in the case of the positive control, which was administered Dox HCl as compared to the negative control group in all tested organs (Fig. 9a). However, a significant ($p < 0.001$) increase of GSH was indicated in TMC-Se-M-NLCs and SeNPs administered groups in the all tested organs, attributed to the enhanced protection of all major organs against oxidative stress, which could be due to SeNPs contained in the lipidic nanoparticle. These enhanced GSH levels help to maintain cellular health and could help to reduce the burden of NF-kB, as well as other inflammatory and pro-inflammatory markers, which could make a substantial impact on HIV replication. Specifically, *in vitro* replication of HIV1 is facilitated by its exposure to oxidative stress [69, 76]. On the other hand, supplementation of anti-oxidant and multivitamins are reported to significantly lower oxidative stress and the HIV1 viral burden [48, 74].

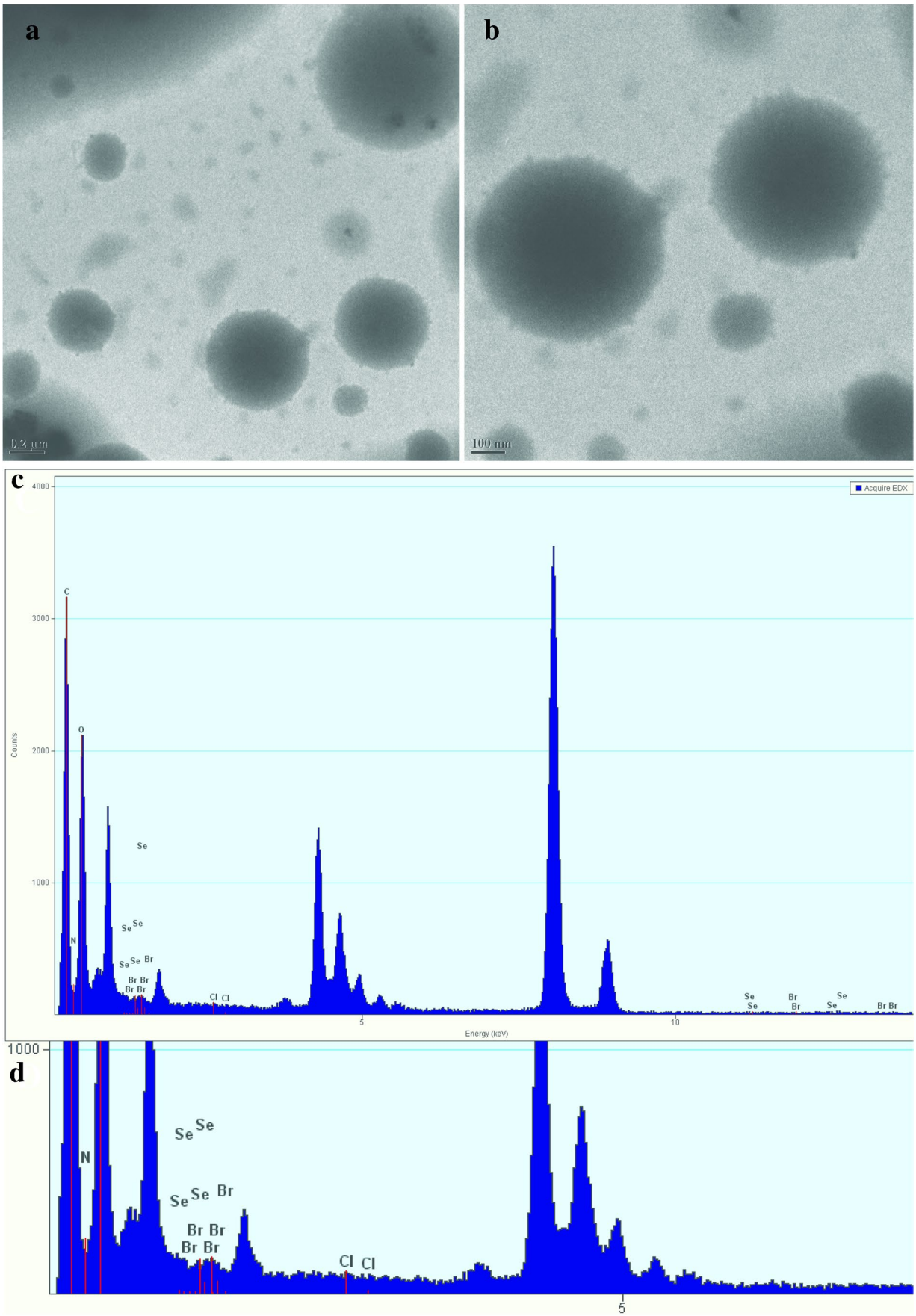
a
0.2 µm
b
100 nm
c
Acquire EDX
Counts
Energy (keV)
C
O
N
Se
Br
Cl
d

◂**Fig. 4** TEM-EDAX images of **a**, **b** TMC-Se-M-NLCs indicating dicrete spherical-shaped nanoparticles (scale bar 200 and 100 nm) **c**, **d** EDAX graph of nano Se-loaded NLCs

### Lipid Peroxidation

Lipid peroxidation (LPO) is an auto-catalytic process that leads to cellular death, and malondialdehyde is the end product in the lipid-peroxidation process [77, 78]. The LPO level was significantly ($p < 0.001$) higher in the positive control than in the negative control, SeNPs, and TMC-Se-M-NLCs administered groups, respectively, in all the tested organs (Fig. 9b). A higher level of LPO was found in the organs such as the heart and liver because of the higher toxicity of the Dox HCl [72, 79]. However, significant ($p < 0.001$) decrease in LPO was found in SeNPs, and TMC-Se-M-NLCs administered groups owing to nanoselenium's chemo-preventive potential [14, 48, 80]. Moreover, TMC-Se-M-NLCs would decrease the peroxidative tissue damage in inflammation, reducing oxidative damage and stress during HIV infection [69, 74, 81].

### Superoxide Dismutase

The superoxide dismutase (SOD) was found to be significantly ($p < 0.001$) lower in the case of a positive control group compared to negative control groups in all tested organs (Fig. 9c). However, SOD values were significantly higher ($p < 0.001$) in all tested organs administered with TMC-Se-M-NLCs and SeNPs than in the positive control. Moreover, selenium-containing nanoformulation could reduce the superoxide radicals; thereby, oxidative damage could subsequently reduce HIV infection pathogenesis and replication [21, 70, 82, 83].

### Catalase

Catalase (CAT) values were significantly ($p < 0.001$) lower in the case of a positive control group administered Dox-HCl than in negative control groups in all the tested organs (Fig. 9d). In contrast, all tested organs from groups administered SeNPs and TMC-Se-M-NLCs exhibited significantly higher ($p < 0.001$) CAT values than the negative control. This could be owing to the chemo-preventive potential of SeNPs shown in Fig. 9d [83]. CAT is a vital intracellular anti-oxidant enzyme that converts the cellular hydrogen peroxide into by-products like water and oxygen, thereby significantly reducing oxidative stress. This reduces the pro-inflammatory cytokines and NF-kB [76], which could help maintain cellular health and reduce HIV infection pathogenesis and replication [21, 82].

### Serum Biochemistry

Liver enzymes such as aspartate transaminase (AST), aminotransferase (ALT), and alkaline phosphatase (ALP) activity level shows normal liver function. The level of AST and ALT, ALP, and total protein was observed to be significantly high ($p < 0.03$) for positive control group administered with the Dox HCl as compared to the negative control groups for all the tested organs because of the toxicity of Dox HCl leading to the cellular damage of liver as shown Fig. 9e [72, 79].

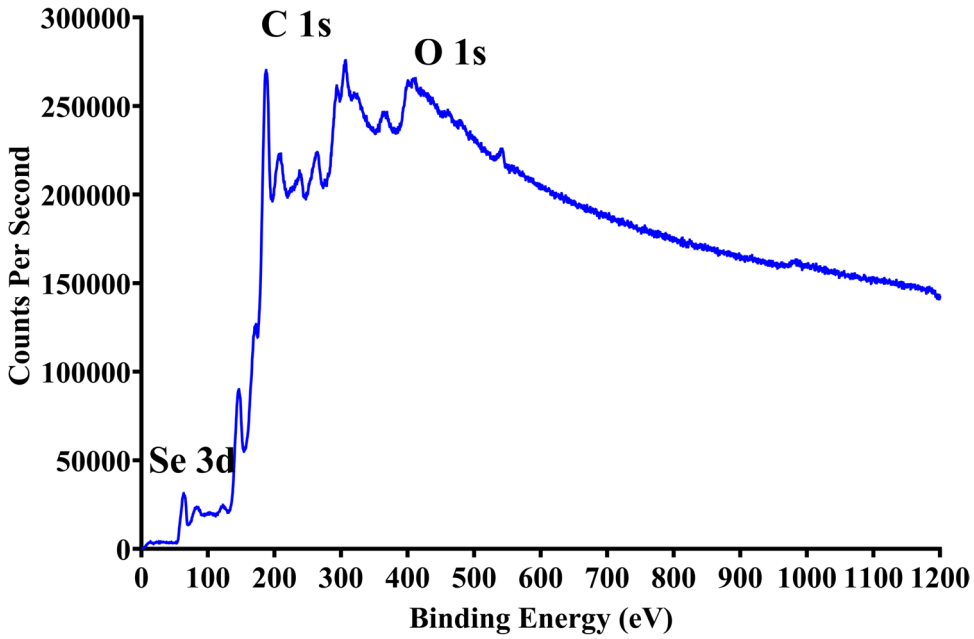


**Fig. 5** XPS spectra of TMC-Se-M-NLCs indicate binding energy concerning the different elements and spectra in 70–48 eV representing a peak for nano Se in the Se3d state

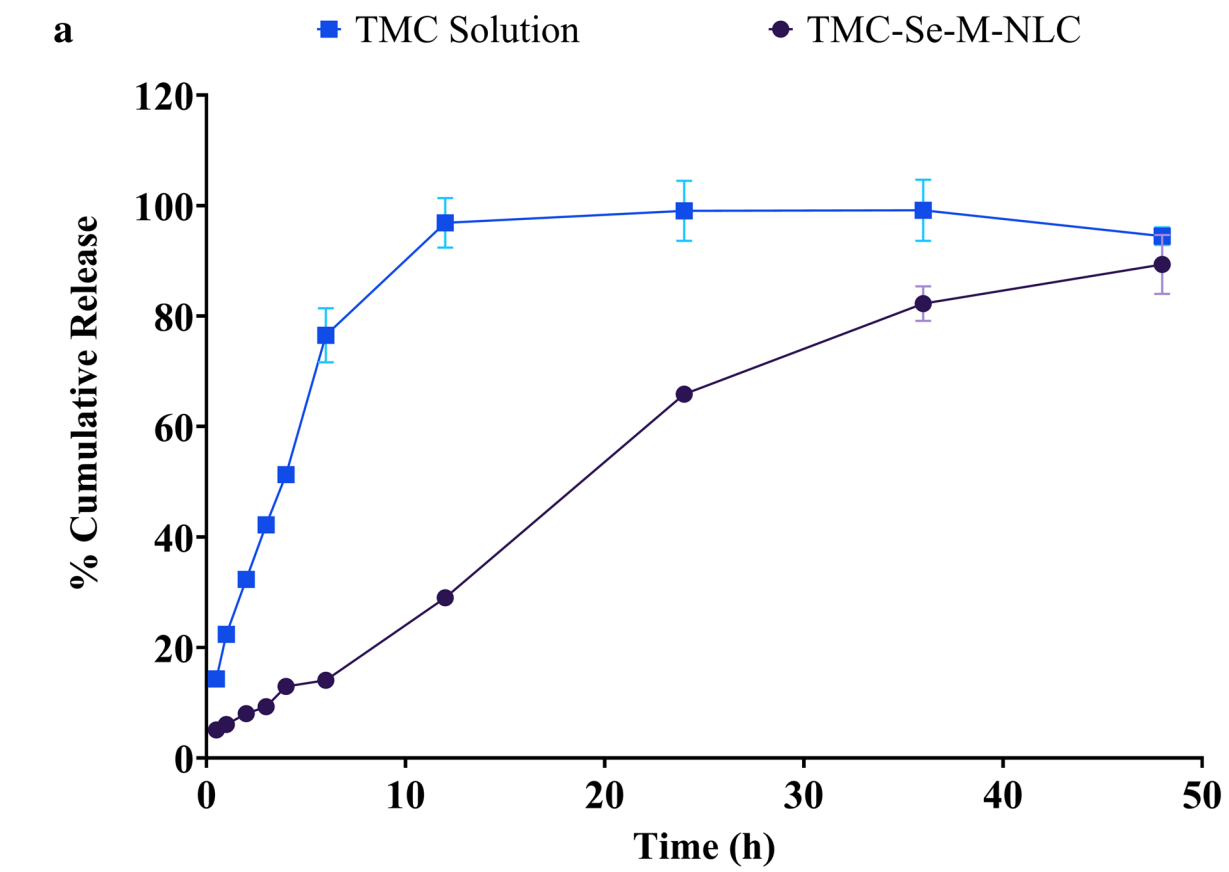
a
TMC Solution
TMC-Se-M-NLC
% Cumulative Release
120
100
80
60
40
20
0
0
10
20
30
40
50
Time (h)

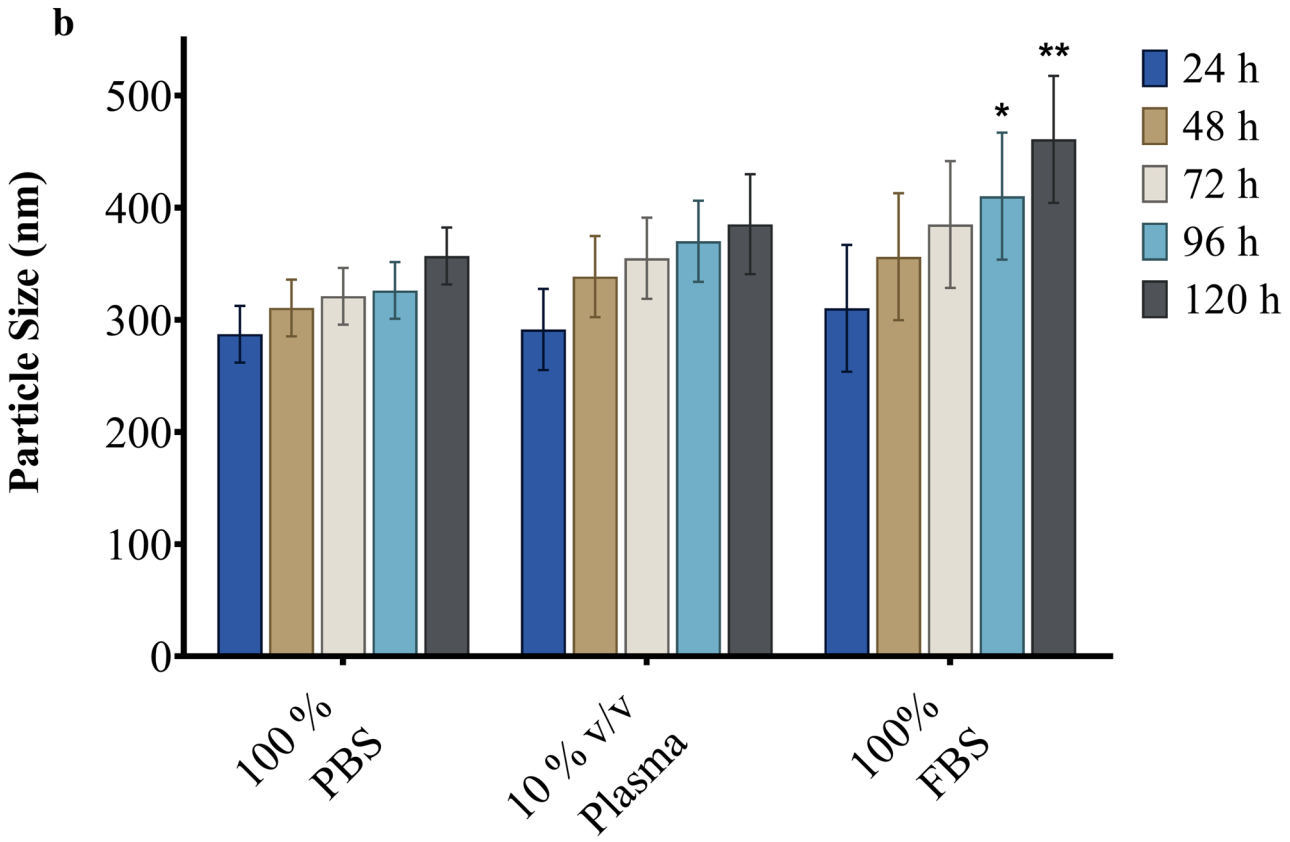
b
Particle Size (nm)
500
400
300
200
100
0
24 h
48 h
72 h
96 h
120 h
*
**
100 % PBS
10 % v/v Plasma
100% FBS

◂**Fig. 6** **a** The drug release of TMC-Se-M-NLCs and TMC solution in (PBS 7.4 and 1% w/v tween 80) (**$p < 0.02$). **b** *In vitro* serum stability study of TMC-Se-M-NLCs with various media such as PBS (100% v/v), plasma (10% v/v) and FBS (100%) (*$p < 0.03$; **$p < 0.009$)

These increased enzymes would indicate cellular oxidative damage in organs [72]. However, ALT, ALP, AST, and total protein values were observed to be significantly lower ($p < 0.001$) in all tested organs of rats administered with TMC-Se-M-NLC and SeNPs as compared to the positive control, which could perhaps be due to the selenium because of its chemo-preventive potential previously reported [21, 80, 84].

## Histopathology

The histopathology of the vital organs is depicted in Fig. 10. The histopathology of all the organs observed for the negative control group appeared normal with no significant changes or differences. However, the histopathology of the organs for the group administered with only the Dox-HCl (positive control) was found to exhibit significant changes, including necrosis, cellular infiltration, and severe degeneration for some of the organs shown in Fig. 10, which is consistent with the well-reported toxicity of Dox-HCl [85]. On the other hand, the sections of the organs for the TMC-Se-M-NLC dosed animals exhibited only minor degeneration even after administration of Dox-HCl compared to positive control, indicating the protective effect of naoselenium encapsulated within the nanostructured lipid carrier system.

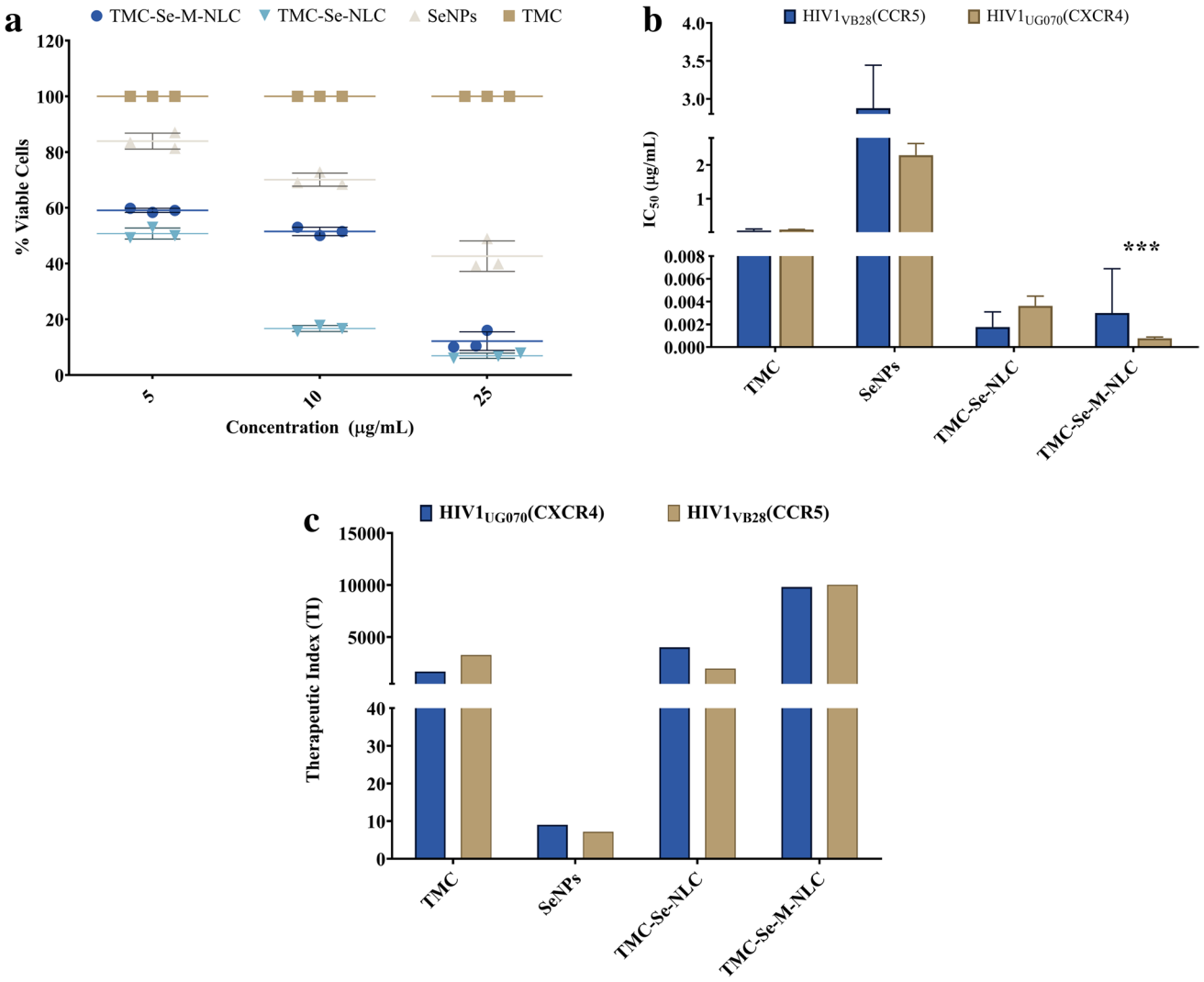


**Fig. 7** **a** The percent viability of TMC, SeNPs and TMC-Se-M-NLCs in TZM-bl cells. **b** $IC_{50}$ values for (TMC, SeNPs and TMC-Se-M-NLCs) when tested for inhibition with $HIV1_{VB28}$ and $HIV1_{UG070}$ virus strains in the TZM-bl cell line. **c** Therapeutic index (TI) of TMC-Se-M-NLCs, TMC, and SeNPs (***$\rho < 0.0001$)

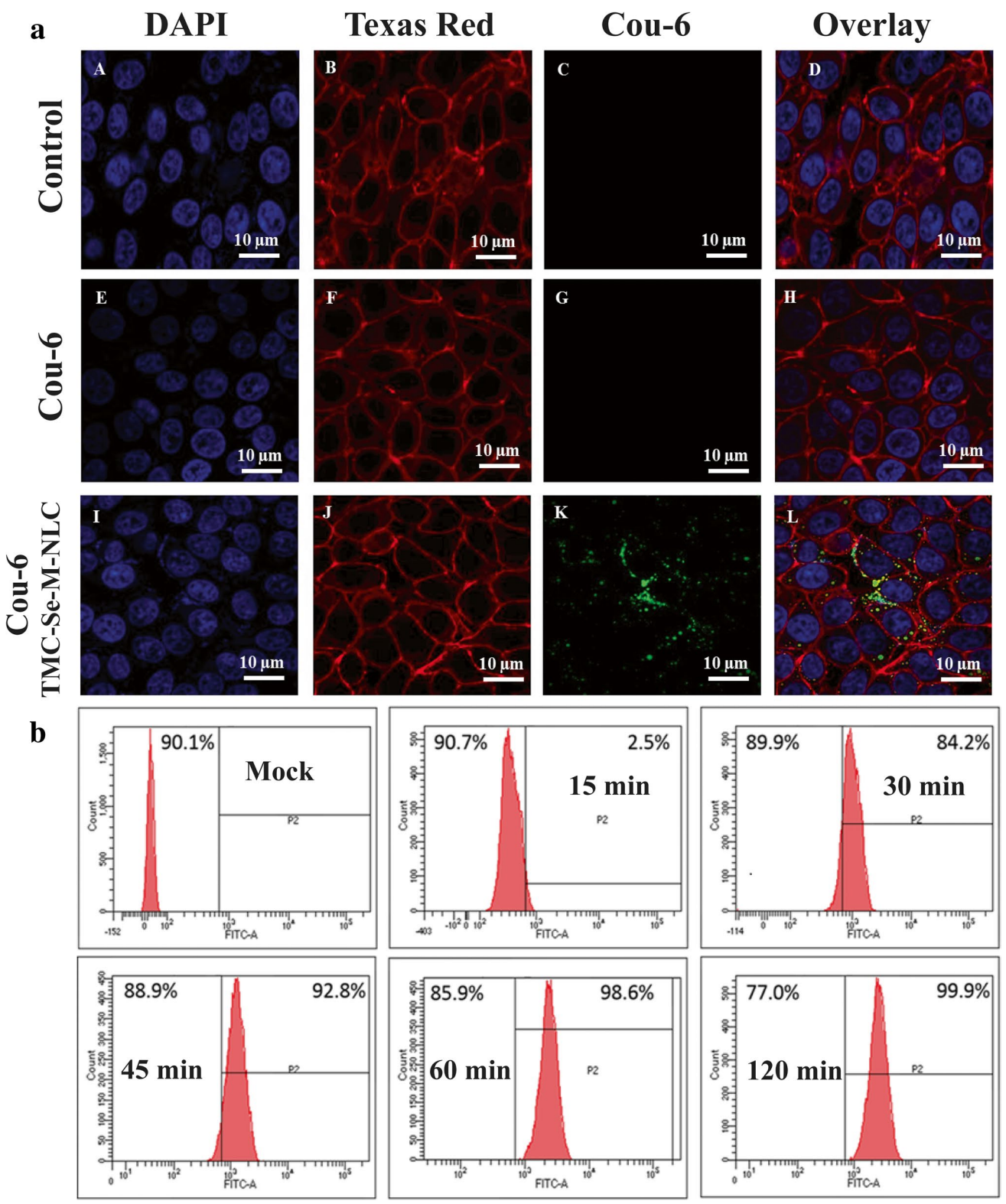


**Fig. 8** **a** Confocal microscopic images representing the internalization of Cou-6 tagged TMC-Se-M-NLCs in TZM-bl, and **b** Coumarin-6 tagged TMC-Se-M-NLCs uptake studies by flow cytometry in TZM-bl cells at 15, 30, 45, 60, and 120 min

### *In vivo* Biodistribution

The biodistribution study was carried out to investigate the efficacy of mannosylated nanoparticles to deliver TMC to the HIV viral reservoir sites. TMC-Se-M-NLCs were observed to accumulate primarily within organs like the kidney, lung, spleen, and liver compared to the TMC solution. The TMC concentration in these organs was significantly higher ($p < 0.003$) in groups administered with TMC-Se-M-NLCs than in the rats administered with TMC solution. The increase in the concentration of TMC at 1 h in the liver was 1.19-fold, in lung 2.13-fold, in kidneys 2.28-fold, and spleen 1.05-fold as than the equivalent dose of TMC solution, as represented in Fig. 11a. This improved TMC concentration could have resulted from a sustained drug release from the mannosylated lipid nanoparticle to the specific sites and its enhanced circulation time in the bloodstream [86, 87]. This could be due to the coat of mannose around the surface of the NLCs, which could be impeding the drug release [33, 79].

Moreover, for the nanocarriers' injected intravenously, pharmacokinetic parameters like the clearance and tissue distribution are more affected by the particle size, surface properties, and opsonization of these nanocarrier systems [50, 88]. Several protein-based proteins/opsonins are adsorbed on the surface of the nanomedicine, consequently facilitating recognition of these particles through the RES systems [89–91]. The RES system is able to absorb various lipid-based nanoformulations, which further improves the drug concentration within the lymphatic system [21, 25, 50, 92–94]. The drug level in anatomical and HIV reservoir sites remarkably increased in the case of mannosylated NLCs.

TMC was not detected at early time points in the brain, ovary, and lymph nodes; however, the level of TMC increased significantly for TMC-Se-M-NLCs administered group at 1 h. The concentration of TMC within the lymph nodes and ovary was 9.83- and 8.05-fold more at 24 h for the groups administered TMC-Se-M-NLCs compared to the groups administered plain TMC solution, as shown in Fig. 11b. This may be due to the particle size range of the nanocarriers along with its lipophilic nature, thereby enabling more RES uptake [50, 89, 94]. This could be explained based on the presence of lectin receptors on HIV viral reservoir sites that favored selective entry of TMC-Se-M-NLCs in the desired areas [33, 79, 95]. It could be most likely that the existence of MR on the macrophages could have fostered this macrophagic uptake [2, 33].

Furthermore, a nearly 12-fold enhancement in the level of TMC in the brain was observed at 1 h for the group administered with mannosylated nanoparticles compared to TMC solution, as shown in Fig. 11b. The brain uptake was enhanced because of the smaller particle size [6, 50]. The RES system and brain absorb the lipid-based nanocarrier because of their lipophilicity and nano size, leading to enhanced intracellular and paracellular transport of such lipid-based nanoparticles across the tight-endothelial junctions of the blood-brain barrier (BBB) [20, 25, 50, 96].

The TMC-Se-M-NLCs could attain appreciable concentration in the several organs where the HIV virus resides. The occurrence of mannose receptors creates an exclusive template, and thus, a multitude of a replica of ligands could be attached to it for facilitating active delivery [2, 36, 79]. Such a strategy could also be beneficial in augmenting the therapeutic effectiveness by lowering the dose of the required bioactive entity and the nanocarriers needed for its delivery [67]. It also showed the synergistic anti-HIV potential and selective cellular uptake, which could help treat HIV synergistically while also improving cellular health by maintaining the intracellular levels of the various anti-oxidants.

## Conclusions

The mannosylated TMC-Se-M-NLCs of Etravirine could be a potential therapeutic approach for efficiently delivering the drug into HIV reservoirs such as the brain, lymph node, and ovaries. The formulation exhibited an enhanced cellular uptake and improved anti-HIV activity in vitro, thereby suggesting its synergistic potential for the treatment of HIV and delivery to HIV reservoirs. The in vitro release demonstrated the controlled release potential of the developed NLC-system, whereas the biodistribution studies indicated the potential of these NLCs to achieve appreciable concentrations in the HIV reservoirs. NLCs offered a promising method to improve the bioavailability of the TMC, BCS class IV drug. This could also be a potential treatment strategy for designing the mannosylated lipid-based nanosystem containing antiretroviral drugs and nano selenium to act more efficiently against HIV infection. It showed the synergistic anti-HIV potential that could act synergistically and thus more efficiently against HIV infection while also improving cellular health by maintaining the intracellular levels of anti-oxidants. However, more studies in humans

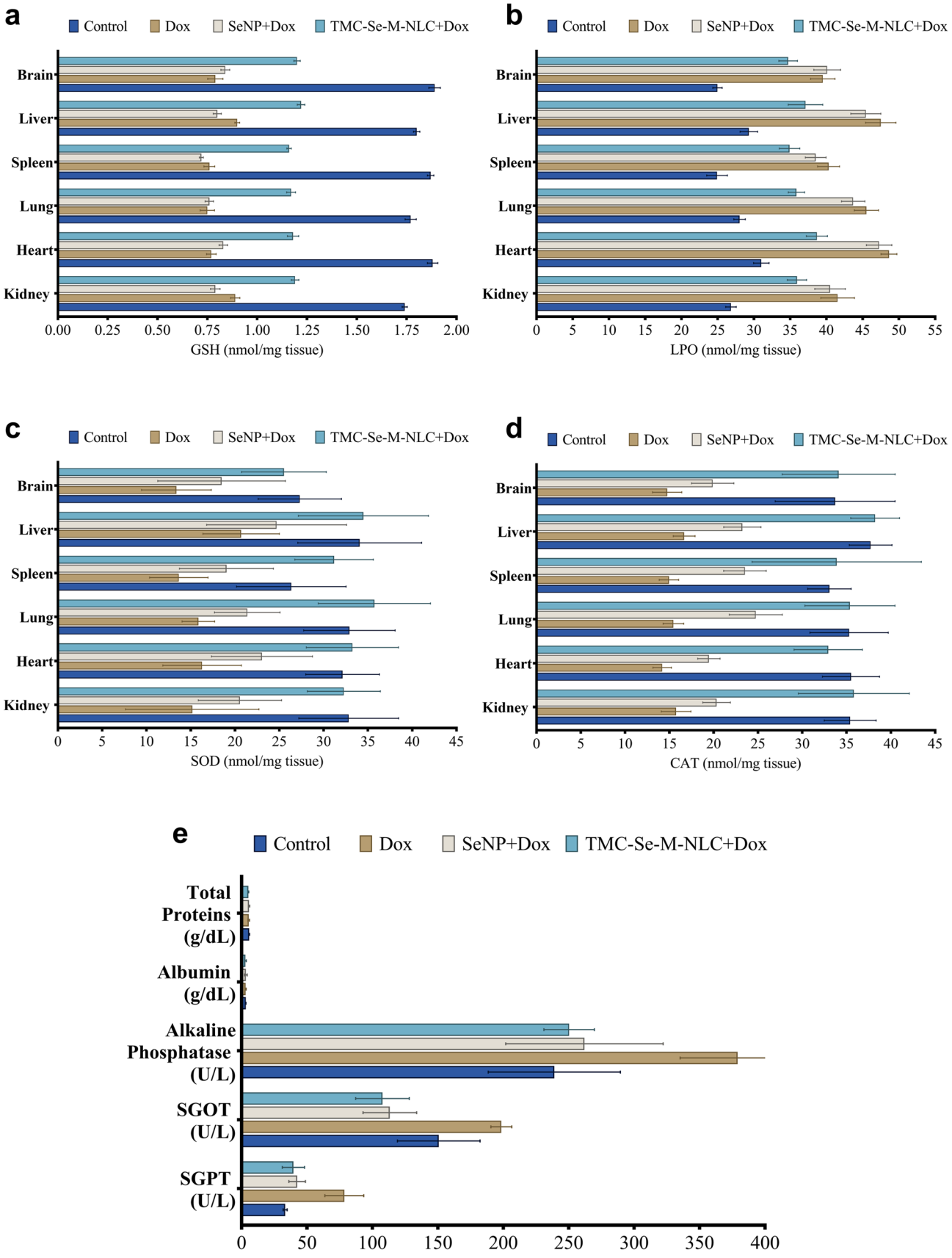
a
Control
Dox
SeNP+Dox
TMC-Se-M-NLC+Dox
Brain
Liver
Spleen
Lung
Heart
Kidney
0.00 0.25 0.50 0.75 1.00 1.25 1.50 1.75 2.00
GSH (nmol/mg tissue)
b
Control
Dox
SeNP+Dox
TMC-Se-M-NLC+Dox
Brain
Liver
Spleen
Lung
Heart
Kidney
0 5 10 15 20 25 30 35 40 45 50 55
LPO (nmol/mg tissue)
c
Control
Dox
SeNP+Dox
TMC-Se-M-NLC+Dox
Brain
Liver
Spleen
Lung
Heart
Kidney
0 5 10 15 20 25 30 35 40 45
SOD (nmol/mg tissue)
d
Control
Dox
SeNP+Dox
TMC-Se-M-NLC+Dox
Brain
Liver
Spleen
Lung
Heart
Kidney
0 5 10 15 20 25 30 35 40 45
CAT (nmol/mg tissue)
e
Control
Dox
SeNP+Dox
TMC-Se-M-NLC+Dox
Total Proteins (g/dL)
Albumin (g/dL)
Alkaline Phosphatase (U/L)
SGOT (U/L)
SGPT (U/L)
0 50 100 150 200 250 300 350 400

◂**Fig. 9** An in-vivo anti-oxidant comparative profile of TMC-Se-M-NLCs, SeNPs, and Dox HCl following intraperitoneal administration of the Dox HCl (5 mg/kg). **a** GSH, nmol/mg tissue, **b** LPO, nmol/mg tissue, **c** SOD, nmol/mg tissue, **d** Catalase, nmol/mg tissue, and **e** serum biochemistry. (*$p < 0.050$, **$p < 0.001$, and NS $p > 0.001$ compared to the control)

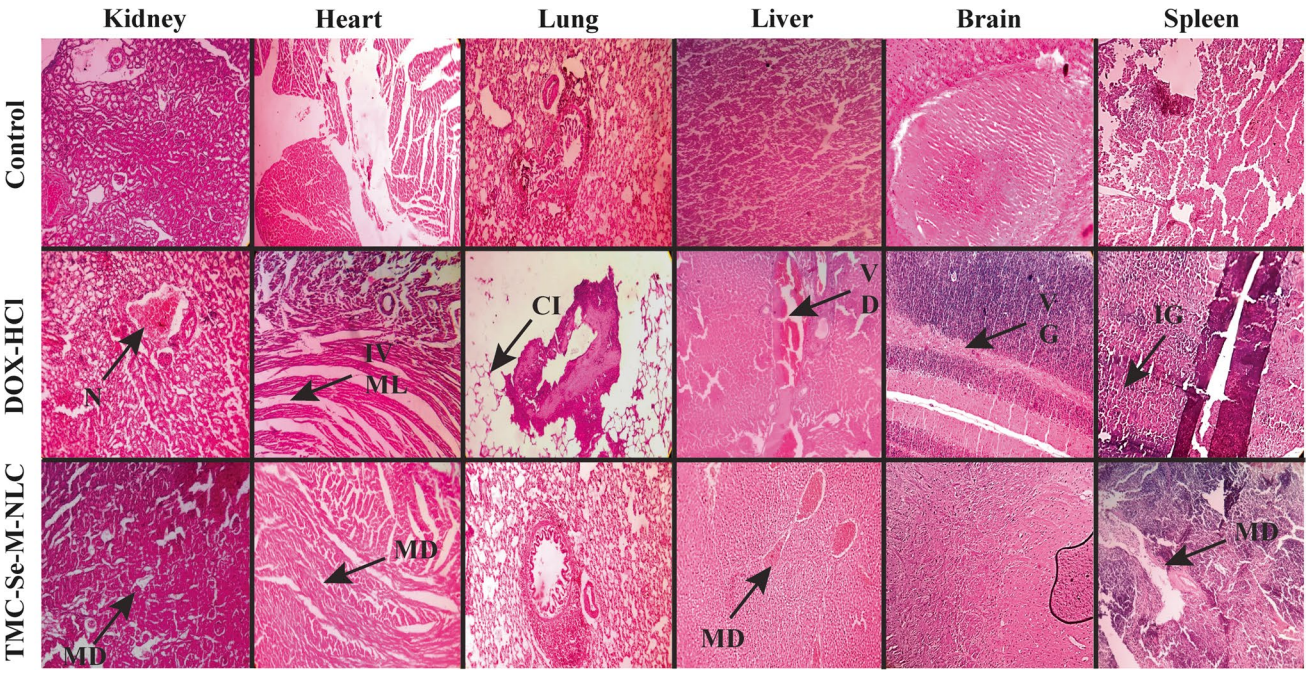


**Fig. 10** Photomicrographs captured at 10× magnification of hematoxylin and eosin-stained sections of the various organs of rats after administration with normal saline (control), DOX-HCl alone TMC-Se-NLC along with DOX-HCl. (*N* necrosis of renal corpuscles, *MD* minor degenerations, *IV* intensive vacuolization, *ML* myofibril loss, *CI* cellular infiltration in the lung, *V* vacuoles, *D* degeneration, *G* gliosis, *IG* increased granulocytes)

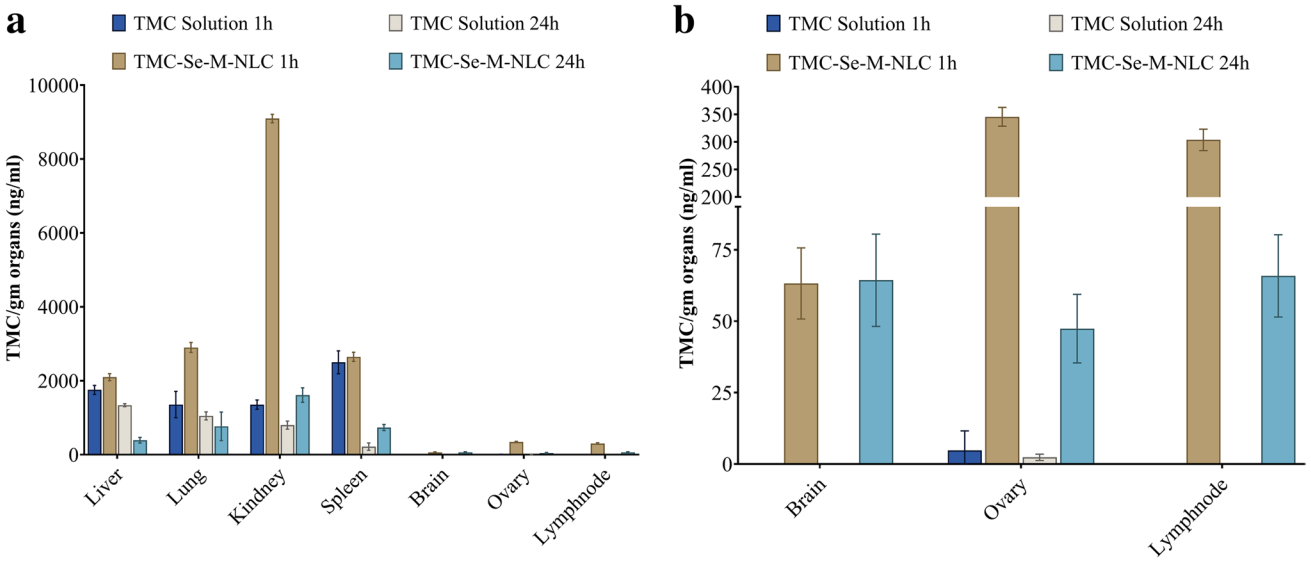


**Fig. 11** **a** Biodistribution profile of 2.5 mg/kg intravenous administration of TMC solution and TMC-Se-M-NLCs in rats at 1 h and 24 h. **b** Zoomed in section of the biodistribution profile showing the distribution in the brain, ovary and lymph nodes. (*$p < 0.05$, one way ANOVA following the unpaired t-test control group in comparison with test groups; $n = 3$ per time point)

are required further to ascertain the capability and potential of lipidic nanocarrier in HIV reservoirs.

**Supplementary Information** The online version contains supplementary material available at https://doi.org/10.1208/s12249-022-02377-8.

**Acknowledgments** The authors are thankful to AICTE-NAFETIC for offering research facilities. The authors also like to thank Dr. V. K Aswal (BARC, Mumbai) for helping in the SANS study. We are thankful to Dr. Samiran Panda (former Director, ICMR-National AIDS Research Institute, Pune, and additional director general, ICMR Headquarters, New Delhi) for performing some parts of the project.

**Author Contribution** Satish V. Rojekar: conceptualization, methodology, data curation, writing—original draft preparation, visualization, investigation, software. Leila Fotooh Abadi: conceptualization, methodology, data curation, writing—original draft preparation, visualization, investigation, software. Rohan Pai: data curation, writing—original draft preparation, writing- review and editing, visualization, software. Mahendra Kumar Prajapati: writing—review and editing, visualization. Smita Kulkarni: supervision, project administration, validation, guidance. Pradeep. R Vavia: Supervision, project administration, validation, guidance, fund acquisition.

**Funding** We would like to acknowledge financial support from the BARTI, Pune, India, BANRF-15-16 and University Grant Commission (RGNF-2017-18-SC-MAH-28486), New Delhi, India by way of fellowship to Satish Rojekar.

## Declarations

**Competing İnterest** The authors declare no competing interests.

## References

1. Mahajan K, Rojekar S, Desai D, Kulkarni S, Bapat G, Zinjarde S, *et al*. Layer-by-layer assembled nanostructured lipid carriers for CD-44 receptor–based targeting in HIV-infected macrophages for efficient HIV-1 inhibition. AAPS PharmSciTech [Internet] 2021 [cited 2021 Jun 24];22:171. Available from: https://doi.org/10.1208/s12249-021-01981-4.
2. Azad AK, Rajaram MVS, Schlesinger LS. Exploitation of the macrophage mannose receptor (CD206) in infectious disease diagnostics and therapeutics. J Cytol Mol Biol [Internet]. 2014;1:1–10 Available from: http://www.ncbi.nlm.nih.gov/pubmed/24672807. http://www.pubmedcentral.nih.gov/articlerender.fcgi?artid=PMC3963702.
3. Garg M, Asthana A, Agashe HB, Agrawal GP, Jain NK. Stavudine-loaded mannosylated liposomes: in-vitro anti-HIV-I activity, tissue distribution and pharmacokinetics. J Pharm Pharmacol Wiley. 2006;58:605–16.
4. Kang X, Wang H, Peng H, Chen B, Zhang W, Wu A, *et al*. Co-delivery of dihydroartemisinin and doxorubicin in mannosylated liposomes for drug-resistant colon cancer therapy. Acta Pharmacol sin 2017 386. Nat Publ Group. 2017;38:885–96.
5. Yu SS, Lau CM, Barham WJ, Onishko HM, Nelson CE, Li H, *et al*. Macrophage-specific RNA interference targeting via "click", mannosylated polymeric micelles. Mol pharm [internet]. Mol Pharm; 2013 [cited 2020 Nov 17];10:975–87. Available from: https://pubmed.ncbi.nlm.nih.gov/23331322/
6. Patel BK, Parikh RH, Patel N. Targeted delivery of mannosylated-PLGA nanoparticles of antiretroviral drug to brain. Int J Nanomedicine. 2018;13:97–100.
7. Han F, Li S, Yin R, Liu H, Xu L. Effect of surfactants on the formation and characterization of a new type of colloidal drug delivery system: nanostructured lipid carriers. Colloids Surfaces A Physicochem Eng Asp. 2008;315:210–6.
8. Mahajan K, Rojekar S, Desai D, Kulkarni S, Vavia P. Ratilal Vavia P. Efavirenz loaded nanostructured lipid carriers for efficient and prolonged viral inhibition in HIV-infected macrophages.
9. Simão DO, Honorato TD, Gobo GG, Piva HL, Goto PL, Rolim LA, *et al*. Preparation and cytotoxicity of lipid nanocarriers containing a hydrophobic flavanone. Colloids Surfaces A Physicochem Eng Asp Elsevier BV. 2020;601:124982.
10. Dan N. Nanostructured lipid carriers: effect of solid phase fraction and distribution on the release of encapsulated materials. Langmuir [Internet]. American Chemical Society;. [cited 2020 Aug 26];30:13809–14. Available from. 2014. https://doi.org/10.1021/la5030197.
11. Kaur CD, Nahar M, Jain NK. Lymphatic targeting of zidovudine using surface-engineered liposomes. J Drug Target. 2008;16:798–805.
12. Fraser IP, Ezekowitz RAB. Mannose receptor and phagocytosis. Adv Cell Mol Biol Membr Organelles JAI. 1999:87–101.
13. Dutta T, Jain NK. Targeting potential and anti-HIV activity of lamivudine loaded mannosylated poly (propyleneimine) dendrimer. Biochim Biophys Acta - Gen Subj. 2007;1770:681–6.
14. Hariharan S, Dharmaraj S. Selenium and selenoproteins: it's role in regulation of inflammation. Inflammopharmacology Springer. 2020:667–95.
15. Baum MK, Campa A, Lai S, Sales Martinez S, Tsalaile L, Burns P, *et al*. Effect of micronutrient supplementation on disease progression in asymptomatic, antiretroviral-naive, HIV-infected adults in Botswana: a randomized clinical trial. JAMA - J Am Med Assoc. 2013;310:2154–63.
16. Dworkin BM. Selenium deficiency in HIV infection and the acquired immunodeficiency syndrome (AIDS). Chem Biol Interact. 1994;91:181–6.
17. Stone CA, Kawai K, Kupka R, Fawzi WW. Role of selenium in HIV infection. Nutr rev [internet]. Nutr Rev; 2010 [cited 2020 Aug 30];68:671–81. Available from: https://pubmed.ncbi.nlm.nih.gov/20961297/
18. Johnson LB, Saravolatz LD. Etravirine, A next-generation non-nucleoside reverse-transcriptase inhbitor. Clin Infect Dis [Internet] 2009 [cited 2020 Feb 26];48:1123–8. Available from: http://www.ncbi.nlm.nih.gov/pubmed/19275497
19. Kakuda TN, De Smedt G, Leemans R, Peeters M, Vyncke V, Van Solingen-ristea R, *et al*. Bioavailability of etravirine 200mg administered as a single 200-mg tablet versus two 100-mg tablets in HIV-negative , healthy volunteers. 2011;20605.
20. John J, Liang D. Oral liquid formulation of etravirine for enhanced bioavailability. J Bioequivalence Bioavailab. 2014;6:46–52.
21. Rojekar S, Pai R, Fotooh Abadi L, Mahajan K, Prajapati M, Kulkarn S, *et al*. Dual loaded nanostructured lipid carrier of Nano-selenium and Etravirine as a potential anti-HIV therapy. Int J Pharm [Internet] Elsevier; 2021 [cited 2021 Aug 12];120986. Available from: https://linkinghub.elsevier.com/retrieve/pii/S0378517321007924
22. Dalvi BR, Shelke RU, Siddiqui EA, Syed AS, Degani MS, *et al*. Preparation , characterization , and surface modification of Nevirapine nanoparticles. Am J Pharmtech Res. 2015;5:187–204.
23. Hollamby MJ. Practical applications of small-angle neutron scattering [Internet]. Phys. Chem. Chem. Phys. The Royal Society of Chemistry; 2013 [cited 2020 Aug 24]. p. 10566–79. Available from: https://pubs.rsc.org/en/content/articlehtml/2013/cp/c3cp50293g

24. Ghosh G, Aswal VK, Varade D. A small angle neutron scattering study on the mixtures of pluronic L121 and anionic surfactant AOT. Pramana - J Phys. 2008;71:1063–7.
25. Rojekar S, Fotooh L, Pai R, Mahajan K, Kulkarni S, Vavia PR. Multi-organ targeting of HIV-1 viral reservoirs with Etravirine loaded nanostructured lipid carrier: an in-vivo proof of concept. Eur J Pharm Sci Elsevier. 2021:105916.
26. Rojekar S, Vora LK, Tekko IA, Volpe-Zanutto F, McCarthy HO, Vavia PR, *et al*. Etravirine-loaded dissolving microneedle arrays for long-acting delivery. Eur J Pharm Biopharm Elsevier BV. 2021;165:41–51.
27. Fotooh Abadi L, Kumar P, Gajbhiye V, Paknikar KM, Kulkarni S. Non-nuke HIV-1 inhibitor shuttled by mesoporous silica nanoparticles effectively slows down HIV-1 replication in infected human cells. Colloids Surfaces B Biointerfaces [Internet]. Elsevier; 2020;194:111227. Available from. https://doi.org/10.1016/j.colsurfb.2020.111227.
28. Ingle SG, Pai RV, Monpara JD, Vavia PR. Liposils: an effective strategy for stabilizing paclitaxel loaded liposomes by surface coating with silica. Eur J Pharm Sci. Elsevier B.V. 2018;122:51–63.
29. Prajapati MK, Pai R, Vavia P. Tuning ligand number to enhance selectivity of paclitaxel liposomes towards ovarian cancer. J Drug Deliv Sci Technol Elsevier. 2021;66:102809.
30. Smith MC, Crist RM, Clogston JD, McNeil SE. Zeta potential: a case study of cationic, anionic, and neutral liposomes. Anal Bioanal Chem [Internet] Springer Verlag; 2017 [cited 2021 Feb 11];409:5779–87. Available from: https://pubmed.ncbi.nlm.nih.gov/28762066/
31. Zuidam NJ, Barenholz Y. Electrostatic parameters of cationic liposomes commonly used for gene delivery as determined by 4-heptadecyl-7-hydroxycoumarin. Biochim Biophys Acta Biomembr. 1997;1329:211–22.
32. Ciani L, Ristori S, Salvati A, Calamai L, Martini G. DOTAP/DOPE and DC-Chol/DOPE lipoplexes for gene delivery: zeta potential measurements and electron spin resonance spectra. Biochim Biophys Acta - Biomembr [internet]. Biochim Biophys Acta; 2004 [cited 2021 Feb 11];1664:70–9. Available from: https://pubmed.ncbi.nlm.nih.gov/15238260/
33. Hatami E, Mu Y, Shields DN, Chauhan SC, Kumar S, Cory TJ, *et al*. Mannose-decorated hybrid nanoparticles for enhanced macrophage targeting. Biochem Biophys Reports Elsevier BV. 2019;17:197–207.
34. Desai J, Thakkar H. Darunavir-loaded lipid nanoparticles for targeting to HIV reservoirs. AAPS PharmSciTech [Internet]. Springer New York LLC; 2018 [cited 2020 Aug 30];19:648–60. Available from: https://pubmed.ncbi.nlm.nih.gov/28948564/
35. Kecili R, Hussain CM. Mechanism of adsorption on nanomaterials. Nanomater Chromatogr Curr trends Chromatogr res Technol tech. Elsevier. 2018:89–115.
36. Rieger J, Freichels H, Imberty A, Putaux JL, Delair T, Jérôme C, *et al*. Polyester nanoparticles presenting mannose residues: toward the development of new vaccine delivery systems combining biodegradability and targeting properties. Biomacromolecules [Internet] American Chemical Society; 2009 [cited 2021 Feb 11];10:651–7. Available from: https://pubs.acs.org/sharingguidelines
37. Araujo VHS, da Silva PB, Szlachetka IO, da Silva SW, Fonseca-Santos B, Chorilli M, *et al*. The influence of NLC composition on curcumin loading under a physicochemical perspective and in vitro evaluation. Colloids surfaces a Physicochem Eng asp. Elsevier BV. 2020;602:125070.
38. Pai RV, Vavia PR. Chitosan oligosaccharide enhances binding of nanostructured lipid carriers to ocular mucins: effect on ocular disposition. Int J Pharm. Elsevier B.V. 2020;577:119095.
39. Zackrisson M, Stradner A, Schurtenberger P, Bergenholtz J. Small-angle neutron scattering on a core-shell colloidal system: a contrast-variation study. Langmuir [Internet]. American Chemical Society ; 2005 [cited 2020 Aug 24];21:10835–45. Available from: https://doi.org/10.1021/la051664v
40. Chen Y, Yang X, Zhao L, Almásy L, Garamus VM, Willumeit R, *et al*. Preparation and characterization of a nanostructured lipid carrier for a poorly soluble drug. Colloids Surfaces A Physicochem Eng Asp. Elsevier B.V. 2014;455:36–43.
41. Sharma PK, Bhatia SR. Effect of anti-inflammatories on Pluronic® F127: micellar assembly, gelation and partitioning. Int J Pharm Elsevier. 2004;278:361–77.
42. Yao HJ, Sun L, Liu Y, Jiang S, Pu Y, Li J, *et al*. Monodistearoylphosphatidylethanolamine-hyaluronic acid functionalization of single-walled carbon nanotubes for targeting intracellular drug delivery to overcome multidrug resistance of cancer cells. Carbon N Y Elsevier Ltd. 2016;96:362–76.
43. Kong H, Yang J, Zhang Y, Fang Y, Nishinari K, Phillips GO. Synthesis and antioxidant properties of gum arabic-stabilized selenium nanoparticles. Int J Biol Macromol Elsevier. 2014;65:155–62.
44. Prasad KS, Selvaraj K. Biogenic synthesis of selenium nanoparticles and their effect on as(III)-induced toxicity on human lymphocytes. Biol trace Elem res [internet]. Biol Trace Elem Res; 2014 [cited 2021 Feb 11];157:275–83. Available from: https://pubmed.ncbi.nlm.nih.gov/24469678/
45. Prasad KS, Vaghasiya J V., Soni SS, Patel J, Patel R, Kumari M, *et al*. Microbial Selenium nanoparticles (SeNPs) and Their application as a sensitive hydrogen peroxide biosensor. Appl Biochem Biotechnol [Internet]. Humana Press Inc.; 2015 [cited 2021 Feb 11];177:1386–93. Available from: https://pubmed.ncbi.nlm.nih.gov/26319569/
46. Chen P, Zhang C, Zhang X, Wang B, Li W, Lei Q. Effects of oxygen plasma treatment power on surface properties of poly(p-phenylene benzobisoxazole) fibers. Appl Surf Sci. 2008;255:3153–8.
47. Pai RV, Monpara JD, Vavia PR. Exploring molecular dynamics simulation to predict binding with ocular mucin: an in silico approach for screening mucoadhesive materials for ocular retentive delivery systems. J Control Release. 2019;309:190–202.
48. Zhang C, Zhai X, Zhao G, Ren F, Leng X. Synthesis, characterization, and controlled release of selenium nanoparticles stabilized by chitosan of different molecular weights. Carbohydr Polym Elsevier Ltd. 2015;134:158–66.
49. Shete H, Patravale V. Long chain lipid based tamoxifen NLC. Part I: Preformulation studies, formulation development and physicochemical characterization. Int J Pharm Elsevier BV. 2013;454:573–83.
50. Jindal AB, Bachhav SS, Devarajan PV. In situ hybrid nano drug delivery system (IHN-DDS) of antiretroviral drug for simultaneous targeting to multiple viral reservoirs: an in vivo proof of concept. Int J pharm [internet]. Elsevier B.V.; 2017;521:196–203. Available from. https://doi.org/10.1016/j.ijpharm.2017.02.024.
51. Aditya NP, Macedo AS, Doktorovova S, Souto EB, Kim S, Chang PS, *et al*. Development and evaluation of lipid nanocarriers for quercetin delivery: a comparative study of solid lipid nanoparticles (SLN), nanostructured lipid carriers (NLC), and lipid nanoemulsions (LNE). LWT - food Sci Technol. Academic Press. 2014;59:115–21.
52. Agrawal P, Gupta U, Jain NK. Glycoconjugated peptide dendrimers-based nanoparticulate system for the delivery of chloroquine phosphate. Biomaterials Elsevier. 2007;28:3349–59.
53. Jain SK, Gupta Y, Jain A, Saxena AR, Khare P, Jain A. Mannosylated gelatin nanoparticles bearing an anti-HIV drug didanosine for site-specific delivery. Nanomed Nanotechnol, Biol Med Elsevier. 2008;4:41–8.

54. Abstiens K, Maslanka Figueroa S, Gregoritza M, Goepferich AM. Interaction of functionalized nanoparticles with serum proteins and its impact on colloidal stability and cargo leaching. Soft Matt Royal Soc Chem. 2019;15:709–20.
55. Mohammad Y, Fallah AB, Reynolds JNJ, Boyd BJ, Rizwan SB. Steric stabilisers govern the colloidal and chemical stability but not in vitro cellular toxicity of linoleoylethanolamide cubosomes. Colloids Surfaces B Biointerfaces Elsevier BV. 2020;192:111063.
56. Doktorovova S, Souto EB, Silva AM. Nanotoxicology applied to solid lipid nanoparticles and nanostructured lipid carriers—a systematic review of in vitro data. Eur. J. Pharm. Biopharm. 2014.
57. Dal Pizzol C, Filippin-Monteiro FB, Restrepo JAS, Pittella F, Silva AH, de Souza PA, *et al*. Influence of surfactant and lipid type on the physicochemical properties and biocompatibility of solid lipid nanoparticles. Int J Environ Res Public Health [Internet] Multidisciplinary Digital Publishing Institute (MDPI). 2014; [cited 2021 Jan 8];11:8581–96. Available from: /pmc/articles/PMC4143879/?report=abstract.
58. Winter E, Pizzol CD, Locatelli C, Crezkynski-Pasa TB. Development and evaluation of lipid nanoparticles for drug delivery: study of toxicity in vitro and in vivo. J Nanosci Nanotechnol. 2016;16:1321–30.
59. Ferro C, Florindo HF, Santos HA. Selenium Nanoparticles for biomedical applications: from development and characterization to therapeutics. Adv Healthc mater. John Wiley & Sons, Ltd; 2021;10:2100598.
60. Steinbrenner H, Al-Quraishy S, Dkhil MA, Wunderlich F, Sies H. Dietary selenium in adjuvant therapy of viral and bacterial infections. Adv Nutr Oxford Acad. 2015;6:73–82.
61. Vieira ACC, Chaves LL, Pinheiro M, Lima SAC, Ferreira D, Sarmento B, *et al*. Mannosylated solid lipid nanoparticles for the selective delivery of rifampicin to macrophages. Artif cells, nanomedicine Biotechnol [internet]. Informa UK limited, trading as Taylor & Francis Group; 2018;46:653–63. Available from. https://doi.org/10.1080/21691401.2018.1434186.
62. Ruge CA, Hillaireau H, Grabowski N, Beck-Broichsitter M, Cañadas O, Tsapis N, *et al*. Pulmonary surfactant protein A-mediated enrichment of surface-decorated polymeric nanoparticles in alveolar macrophages. Mol Pharm [Internet] American Chemical Society; 2016 [cited 2021 Jun 24];13:4168–78. Available from: https://pubmed.ncbi.nlm.nih.gov/27934478/
63. Barros D, Lima SAC, Cordeiro-Da-Silva A. Surface functionalization of polymeric nanospheres modulates macrophage activation: relevance in Leishmaniasis therapy. Nanomedicine [Internet] Future Medicine Ltd; 2015 [cited 2021 Jun 24];10:387–403. Available from: https://pubmed.ncbi.nlm.nih.gov/25707974/
64. Behzadi S, Serpooshan V, Tao W, Hamaly MA, Alkawareek MY, Dreaden EC, *et al*. Cellular uptake of nanoparticles: journey inside the cell. Rev: Chem. Soc; 2017.
65. Sabourian P, Yazdani G, Ashraf SS, Frounchi M, Mashayekhan S, Kiani S, *et al*. Effect of physico-chemical properties of nanoparticles on their intracellular uptake. Int J Mol Sci. 2020;21:1–20.
66. Khoury R, Grysman N, Gold J, Patel K, Grossberg GT. The role of 5 HT6-receptor antagonists in Alzheimer's disease: an update. Expert Opin Investig Drugs Taylor & Francis. 2018;27:523–33.
67. Saraogi GK, Sharma B, Joshi B, Gupta P, Gupta UD, Jain NK, *et al*. Mannosylated gelatin nanoparticles bearing isoniazid for effective management of tuberculosis. J Drug Target. 2011;19:219–27.
68. Malik T, Chauhan G, Rath G, Kesarkar RN, Chowdhary AS, Goyal AK. Efaverinz and nano-gold-loaded mannosylated niosomes: a host cell-targeted topical HIV-1 prophylaxis via thermogel system. Artif Cells, Nanomedicine Biotechnol [Internet] Taylor and Francis Ltd; 2018 [cited 2020 Nov 17];46:79–90. Available from: https://pubmed.ncbi.nlm.nih.gov/29231058/
69. Stone CA, Kawai K, Kupka R, Fawzi WW. The role of selenium in HIV infection cosby a stone, Kosuke Kawai, Roland Kupka, Wafaie W Fawzi Harvard School of Public Health. Nutr Rev [Internet]. 2010;68:671–81 Available from: http://www.ncbi.nlm.nih.gov/pmc/articles/PMC3066516/.
70. Santoro MG, Rossi A, Amici C. NF-κB and virus infection: who controls whom [internet]. EMBO J. John Wiley & Sons, ltd; 2003 [cited 2021 Feb 11]. p. 2552–60. Available from. https://doi.org/10.1093/emboj/cdg267.
71. Rezvanfar MA, Rezvanfar MA, Shahverdi AR, Ahmadi A, Baeeri M, Mohammadirad A, *et al*. Protection of cisplatin-induced spermatotoxicity, DNA damage and chromatin abnormality by selenium nano-particles. Toxicol Appl Pharmacol. 2013;266:356–65.
72. Diamanti J, Mezzetti B, Giampieri F, Alvarez-Suarez JM, Quiles JL, Gonzalez-Alonso A, *et al*. Doxorubicin-induced oxidative stress in rats is efficiently counteracted by dietary anthocyanin differently enriched strawberry (Fragaria × ananassa Duch.). J Agric Food Chem. 2014;62:3935–43.
73. Hoffmann PR, Berry MJ. The influence of selenium on immune responses [internet]. Mol. Nutr. Food res. John Wiley & Sons, ltd; 2008 [cited 2020 Aug 30]. p. 1273–80. Available from. https://doi.org/10.1002/mnfr.200700330.
74. Pitney CL, Royal M, Klebert M. Selenium supplementation in HIV-infected patients: is there any potential clinical benefit? J Assoc Nurses AIDS Care. 2009;20:326–33.
75. Neamat-Allah ANF, Mahmoud EA, Abd El Hakim Y. Efficacy of dietary nano-selenium on growth, immune response, antioxidant, transcriptomic profile and resistance of Nile tilapia, Oreochromis niloticus against streptococcus iniae infection. Fish Shellfish Immunol Academic Press. 2019;94:280–7.
76. Guillin OM, Vindry C, Ohlmann T, Chavatte L. Selenium, selenoproteins and viral infection. MDPI AG: Nutrients; 2019.
77. Liu J, Meng J, Cao L, Li Y, Deng P, Pan P, *et al*. Synthesis and investigations of ciprofloxacin loaded engineered selenium lipid nanocarriers for effective drug delivery system for preventing lung infections of interstitial lung disease. J Photochem Photobiol B biol [internet]. Elsevier; 2019;197:111510. Available from. https://doi.org/10.1016/j.jphotobiol.2019.05.007.
78. Alam MN, Bristi NJ, Rafiquzzaman M. Review on in vivo and in vitro methods evaluation of antioxidant activity. Saudi Pharm J [Internet]. 2013;21:143–52. Available from. https://doi.org/10.1016/j.jsps.2012.05.002.
79. Jain A, Agarwal A, Majumder S, Lariya N, Khaya A, Agrawal H, *et al*. Mannosylated solid lipid nanoparticles as vectors for site-specific delivery of an anti-cancer drug. J Control Release Elsevier. 2010;148:359–67.
80. Dehkordi AJ, Mohebbi AN, Aslani MR, Ghoreyshi SM. Evaluation of nanoselenium (Nano-se) effect on hematological and serum biochemical parameters of rat in experimentally lead poisoning. Hum Exp Toxicol [internet]. SAGE Publications Ltd. 2017; [cited 2020 Dec 30];36:421–7. Available from: https://pubmed.ncbi.nlm.nih.gov/27251766/.
81. Nasirpour M, Sadeghi AA, Chamani M. Effects of nano-selenium on the liver antioxidant enzyme activity and immunoglobolins in male rats exposed to oxidative stress. J Livest Sci. 2017;8:81–7.
82. Kostyushov V V., Bokal II, Petrov SA. The study of activity of blood antioxidant enzymes in HIV infection. Biochem Suppl Ser B Biomed Chem [Internet]. Springer; 2011 [cited 2021 Feb 11];5:193–6. Available from: https://doi.org/10.1134/S1990750811020041
83. Watanabe LM, Barbosa Júnior F, Jordão AA, Navarro AM. Influence of HIV infection and the use of antiretroviral therapy on selenium and selenomethionine concentrations and antioxidant protection. Nutrition Elsevier Inc. 2016;32:1238–42.
84. Messarah M, Klibet F, Boumendjel A, Abdennour C, Bouzerna N, Boulakoud MS, *et al*. Hepatoprotective role and antioxidant capacity of selenium on arsenic-induced liver injury in rats. Exp Toxicol Pathol. 2012;64:167–74.

85. Yokaichiya F, Schmidt C, Storsberg J, Kumpugdee Vollrath M, de Araujo DR, Kent B, *et al*. Effects of doxorubicin on the structural and morphological characterization of solid lipid nanoparticles (SLN) using small angle neutron scattering (SANS) and small angle X-ray scattering (SAXS). Phys B Condens Matter North-Holland. 2018;551:191–6.
86. Joshi M, Pathak S, Sharma S, Patravale V. Design and in vivo pharmacodynamic evaluation of nanostructured lipid carriers for parenteral delivery of artemether: Nanoject. Int J Pharm. 2008;364:119–26.
87. Spinks CB, Zidan AS, Khan MA, Habib MJ, Faustino PJ. Pharmaceutical characterization of novel tenofovir liposomal formulations for enhanced oral drug delivery: in vitro pharmaceutics and Caco-2 permeability investigations. Clin Pharmacol Adv Appl. 2017;9:29–38.
88. Sakai-Kato K, Yoshida K, Izutsu K ichi. Effect of surface charge on the size-dependent cellular internalization of liposomes. Chem Phys Lipids Elsevier Ireland Ltd; 2019;224.
89. Kulkarni SA, Feng SS. Effects of particle size and surface modification on cellular uptake and biodistribution of polymeric nanoparticles for drug delivery. Pharm Res. 2013;30:2512–22.
90. Makabi-Panzu B, Lessard C, Perron S, Désormeaux A, Tremblay M, Poulin L, *et al*. Comparison of cellular accumulation, tissue distribution, and anti-HIV activity of free and liposomal 2′,3′-dideoxycytidine. AIDS Res Hum Retrovir. 1994;10:1463–70.
91. Moghimi SM, Patel HM. Tissue specific opsonins for phagocytic cells and their different affinity for cholesterol-rich liposomes. FEBS Lett. 1988;233:143–7.
92. Poovi G, Damodharan N. Lipid nanoparticles: a challenging approach for oral delivery of BCS class-II drugs. Futur J Pharm Sci Springer Science and Business Media LLC. 2018;4:191–205.
93. Zhang W, Liu J, Zhang Q, Li X, Yu S, Yang X, *et al*. Enhanced cellular uptake and anti-proliferating effect of chitosan hydrochlorides modified genistein loaded NLC on human lens epithelial cells. Int J Pharm. Elsevier. 2014;471:118–26.
94. Soni M, Shelkar N, Gaikwad R, Vanage G, Samad A, Devarajan P. Buparvaquone loaded solid lipid nanoparticles for targeted delivery in theleriosis. J Pharm Bioallied Sci [Internet] Medknow Publications. 2014; [cited 2020 Aug 26];6:22–30. Available from: /pmc/articles/PMC3895290/?report=abstract.
95. Vieira ACC, Magalhães J, Rocha S, Cardoso MS, Santos SG, Borges M, *et al*. Targeted macrophages delivery of rifampicin-loaded lipid nanoparticles to improve tuberculosis treatment. Nanomedicine. 2017;12:2721–36.
96. Tiraboschi JM, Niubo J, Vila A, Perez-Pujol S, Podzamczer D. Etravirine concentrations in CSF in HIV-infected patients. J Antimicrob Chemother. 2012;67:1446–8.